Optimization of topical delivery for niacinamide using hydrogels and transethosomes for anti-ageing effect

Renata da Costa Alves Basto

Dissertation for the Degree of Master of Science in Bioengineering at the Faculdade de Engenharia and Instituto Ciências Biomédicas Abel Salazar da Universidade do Porto

Supervisors: Dr Sofia Lima and Dr Cláudia Nunes

March 2021

© Renata Basto, 2021

Follow the evidence wherever it leads, and question everything.

- Neil deGrasse Tyson

Acknowledgments

I would like to acknowledge all the people who played a role in this adventure.

Prof Salette Reis, first of all, I want to thank you for the opportunity to let me be a part of this group. When I first contacted you, I was taken aback by the lovely hospitality, and I was far from imagining the amazing journey that I would have in front, full of interesting challenges.

Dr Sofia Lima and Dr Cláudia Nunes, you were the driving force of my work. It was a pleasure to learn from you, especially what does not come in any book. To learn that the only solution for a failure is to put on our lab coat and try again. You were always available to guide me when I needed to, teaching me how important it is to know how to reinvent the narrative, always looking after my interest, in the best way possible.

To **Raquel Andrade**, you were, without a doubt, my lab buddy. I am beyond grateful for all the time you spent helping and guiding me, even when it meant staying late in the lab. For all the moments of laughter and motivation you gave me, thank you.

To **Ana Isabel**, for being one of the most helpful and dearest people I have ever met. Thank you for being one-whatsapp away whenever I needed and for always transmitting me calm.

To **all the members of the research group**, whom, in one way or another, made me feel welcomed, accompanied me during these months and helped me when I needed it.

To my **friends**, for being my escape and, most importantly, for pretending to be interested in hydrogels and nanoparticles.

To my **grandparents**, who despite not understanding much of the topic, asked me every week how it was going.

Last, but definitely not least, to my **parents and sister**, for your constant support, love and motivation, not just throughout this study, but also in life. Thank you for making me believe in myself (and for bringing me chocolates when my brain needed it most).

Index

Abstract **9**

1. Introduction **11**

1.1. Skin 11

1.1.1. Function 11

1.1.2. Structure 12

1.2. Topical Delivery 13

1.2.1. Topical Versus Transdermal Drug Delivery: Understanding Differences 14

1.2.2. Drug permeation pathways in the skin 15

1.3. Factors affecting drug permeation 16

1.3.1. Physiological properties of the skin 16

1.3.2. Physicochemical properties of the drug 18

1.4. Niacinamide 19

1.5. Ageing 21

1.5.1. The treatment of ageing with NIA 22

1.6. Drug Delivery Systems 22

1.6.1. Hydrogels 23

1.6.2. Nanocarriers 24

2. Motivation **27**

3. Materials and Methods **28**

3.1. Materials and Instrumentation 28

3.2. Preparation and Optimization of Drug Delivery Systems 28

3.2.1. Preparation of carrageenan-polyvinylpyrrolidone hydrogels 28

3.2.2. Optimization of carrageenan hydrogels 29

3.2.3. Preparation of transethosome formulations 29

3.2.4. Transethosomes-loaded hydrogels 31

3.3. Characterization Techniques of Hydrogels and Transethosomes 31

3.3.1. Fourier-transform infrared spectroscopy evaluation 31

3.3.2. Morphological analysis 31

3.3.3. Swelling assay 32

3.3.4. Transethosomes vesicles size, polydispersity index and zeta potential 32

3.3.5. Analytical method 32

3.3.6. Determination of the entrapment efficiency and drug loading capacity 33

3.3.7. Stability studies 34

3.4. *In Vitro* Permeation Studies 34
3.4.1. Skin Preparation 34
3.4.2. *In vitro* skin diffusion studies 34
3.5. Statistical Analysis 35
4. Results and Discussion 36
4.1. Validation of HPLC method for Niacinamide 36
4.1.1. Purpose of validation 36
4.1.2. Chromatographic conditions 36
4.1.3. Validation parameters 37
4.1.4. Standard and sample preparations 37
4.1.5. Linearity and range 37
4.1.6. Limit of quantification and Limit of Detection 38
4.1.7. Accuracy and Precision 39
4.2. Hydrogels 40
4.2.1. Optimization of carrageenan-based hydrogels 40
4.2.2. Fourier-transform infrared spectroscopy evaluation 43
4.2.3. Morphology evaluation 45
4.2.4. Swelling 48
4.2.5. *In vitro* permeation assay 49
4.3. Transethosomes 50
4.3.1. Formulation and characterization of transethosomes 50
4.3.2. Fourier-transform infrared spectroscopy evaluation 52
4.3.3. Morphology evaluation 54
4.3.4. Stability assessment 54
4.3.5. *In vitro* permeation assay 56
4.4. Transethosomes-loaded hydrogels 57
4.5. Apparent Permeability Comparison 58
5. Concluding remarks 59
6. References 62
7. Supplementary Figures 70

List of figures

Figure 1 - Topical versus transdermal delivery across the skin layers. 14

Figure 2 - Permeation pathways in the skin.. 15

Figure 3 - Representative image of the structural composition of conventional liposomes, ethosomes, transferosomes and transethosomes. 25

Figure 4 - Transethosome formulation via thin film method. 30

Figure 5 - Franz diffusion cell system. 35

Figure 6 - Line regression graph of niacinamide. 38

Figure 7 - List and photograph of hybrid hydrogels. 41

Figure 8 – List and photographs of final hydrogel combinations.. 42

Figure 9 - The FTIR spectra of CRG-PVP NIA-loaded hydrogel (Type A) and all reference compounds. 43

Figure 10 - Schematic representation of hydrogen bonding interactions in the CRG-PVP hydrogel. 44

Figure 11 - Evaluation of JO effect on NIA-loaded hydrogel's chemical nature through FTIR. 45

Figure 12 - Morphology of CRG-PVP hydrogel matrix. 46

Figure 13 – Influence of JO in hydrogels morphology by SEM. 47

Figure 14 – Photograph of JO hydrogels swelling behavior under neutral salt and basic conditions. 48

Figure 15 - *In vitro* skin permeation results of free NIA, and NIA-loaded developed hydrogels. 49

Figure 16 - The FTIR spectra of reference compound (NIA) and nanoformulations (Type I and Type I w/ NIA). 53

Figure 17 - FTIR spectra of Type I, II, and III formulations, containing NIA. 53

Figure 18 - Non-loaded and NIA-loaded TEs morphology. 54

Figure 19 - Storage stability of NIA-loaded formulations at 4ºC over 2 weeks. 55

Figure 20 - Storage stability of NIA-loaded formulations at 4ºC over 8 weeks. EE% and LC% values displayed. 55

Figure 21 – *In vitro* skin permeation results of free NIA, and NIA-loaded TEs (Type I, II, and III). 56

Figure 22 - *In vitro* skin permeation results of free NIA, NIA-loaded hydrogel, and TEs-loaded hydrogels (Type I, II, and III). 57

List of supplementary figures

Figure S1 – Hydrogels with different CRG amounts, 0.90% and 1% (w/v) 70

Figure S2 – Artifacts on the surface of CRG-PVP hydrogel matrix..... 70

Figure S3 - JO silk-like effect on CRG-PVP hydrogel macrostructure..... 70

Figure S4 - The FTIR spectra of reference compound (NIA) and nanoformulations (Type II and Type II w/ NIA). 71

Figure S5 - The FTIR spectra of reference compound (NIA) and nanoformulations (Type III and Type III w/ NIA)..... 71

Figure S6 - Storage stability of non-loaded formulations at 4ºC over 2 weeks..... 72

List of tables

Table 1 - Physicochemical properties of NIA..... 20

Table 2 - Optimized carrageenan hydrogels with different compositions 29

Table 3 - The composition of four hydrogels with different JO percentages 29

Table 4 - The composition of transethosomes..... 29

Table 5 - Chromatographic conditions..... 36

Table 6 - Linearity results of niacinamide 38

Table 7 - Accuracy and precision for intra-day variability..... 39

Table 8 - Accuracy and precision for inter-day variability..... 40

Table 9 - Characterization of non-loaded TEs Type I, II, and III. 51

Table 10 - Characterization of loaded-TEs Type I, II, and III. 52

Table 11 - Apparent permeability coefficient of Free NIA and NIA-loaded formulations across the *in vitro* skin barrier 58

Acronyms and abbreviations

3D	Three-dimensional
ATR	Attenuated Total Reflectance
CEs	Chemical Enhancers
CRG	Carrageenan
CV	Coefficient variation
EDC	1-ethyl-3-(3-dimethylaminopropyl) carbodiimide hydrochloride
EE	Entrapment efficiency
EPC	Egg yolk phosphatidylcholine
F	Formulations
FTIR	Fourier Transform Infrared Spectroscopy
GI	Gastrointestinal
HEPES	4-(2-hydroxyethyl)-1-piperazineethanesulfonic acid
HPLC	High-performance liquid chromatography
JO	Jojoba oil
LC	Loading Capacity
LOD	Limit of Detection
LOQ	Limit of Quantification
NHS	N-hydroxysuccinimide
NIA	Niacinamide
NPs	Nanoparticles
P_{app}	Apparent Permeability
PBS	Phosphate-buffered saline
PDI	Polydispersity index
PEs	Permeation enhancers
PS	Particle Size
PVP	Polyvinylpyrrolidone

PVA	Polyvinyl alcohol
ROS	Reactive Oxygen Species
S	Sulfur
SAA	Surface Active Agent
SC	*stratum corneum*
SEM	Scanning Electron Microscopy
SR	Swelling Ratio
TE	Transethosome
TEM	Transmission Electron Microscopy
TPP	Tripolyphosphate
UV	Ultraviolet
ZP	Zeta Potential

Symbols

Categorization of CRG:

κ	Kappa
ι	Iota
λ	Lambda
μ	Um
ν	Nu
θ	Theta

Abstract

Niacinamide (NIA) is an amide form of vitamin B3, and a water-soluble molecule, that is suitable for use in skin disorders, and in abrogating features of ageing, by acting as an antioxidant and preventing dehydration. If topical delivery is needed, some niacinamide's physicochemical properties suggest that this bioactive compound may have difficulties to surpass the barrier imposed by *stratum corneum*. Therefore, the aim of this study was to formulate NIA into two drug delivery systems to enhance its absorption and controlled permeation across the skin layers. The ones designed and characterized in this research work were hydrogels and transethosomes (TEs).

Optimization of carrageenan (CRG) based hydrogels composition led to the design of three formulations with polyvinylpyrrolidone (PVP). They differed only in the amount of jojoba oil (JO) present; the permeation enhancer selected for this delivery system. All CRG-PVP hydrogels exhibited a porous and highly aligned macrostructure, and when present, JO was clearly detectable in their morphology. Fourier transform infrared spectroscopy (FTIR) validated the presence of both polymers in the hydrogel matrix, as well as, the incorporation of NIA. Swelling assay did not result in the expansion of the hydrogel, as a syneresis phenomenon must have taken place instead. Although there were no significant differences in the permeation capacity between the different hydrogels used, with distinct JO amounts, after 6 h, it was possible to observe a permeation rate of about 40%.

Designing of TEs led to the production of three different formulations, with distinct surface-active agents; Tween-80 for Type I, oleic acid for Type II, and JO for Type III. Formulations were characterized by performing measurements of size, polydispersity index, zeta potential, encapsulation efficiency and loading capacity, and by evaluating chemical interactions (FTIR) and morphology. Although they presented an ideal hydrodynamic size range for topical delivery, TEs showed low encapsulation efficiency (≤ 6%) and loading capacity (≤ 10%) values. Niacinamide was successfully incorporated into the TEs, without altering their chemical structure and morphology. During storage at 4ºC, Type II TEs proved to be the least stable ones, as their NIA content decreased to half in two weeks. *In vitro* permeation assays with transethosomes showed that these nanoparticles are more effective at retaining NIA in the skin, comparing to NIA-loaded hydrogels, which penetrate and permeate more easily. After 6 h, TEs showed a cumulative permeation rate of about 20% for Type I and Type III, and 10% for Type II, practically half of the results obtained with hydrogels.

Skin permeation studies with TEs-loaded hydrogels showed that the combination of the two drug delivery systems resulted in an adequate controlled permeation of NIA. After 6 h, TEs-loaded hydrogels showed a cumulative permeation ranging from 10 – 30 %.

Given the consistency and storage stability of the TEs incorporated within CRG-PVP hydrogels, the NIA permeated and the apparent permeability (P_{app}) values calculated, the combination of the hydrogel with TEs Type III is the best option, for the topical anti-ageing effect intended.

1. Introduction

1.1. Skin

To properly assess and rationalize the ability of a drug to be delivered in the skin, an understanding of the fundamental aspects of skin anatomy and physiology is of crucial importance and will be firstly discussed in this section.

1.1.1. Function

The skin accounts for about 15 % of the total body weight of an adult and has a surface area of 1.5 – 2 m^2, making it the largest organ in the human body[1].

As the largest component of the integumentary system, skin establishes the interface between the outside environment and the body's internal living tissues and organs, ensuring a protective barrier against physical, chemical, biological, radiological, and thermal damages[2].

Skin is an archetype of organs involved in mechanical and immunological barriers to pathogens[3,4]. Given that many physical, chemical, and microbial insults affect the skin, several types of immune cells reside in or are recruited into the different layers of the skin to maintain homeostasis upon multiple stresses, such as wounding and infection[5,6]. This immunological network is in a symbiotic relationship with the millions of commensal bacteria, fungi, and viruses that compose the skin microbiota[3,5]. Similar to those in our gut, skin microorganisms occupy a wide range of skin niches and have fundamental and beneficial roles in the protection against invading pathogens and in the education of the immune system[7,8].

The skin also serves important metabolic and sensorial functions. It reduces harmful effects of temperature deregulation and ultraviolet (UV) radiation by expressing UV-absorbing molecules, including melanin, trans-urocanic acid, vitamin D and C metabolites, and heat-shock proteins[2]. Additionally, skin harbors specialized nerve networks that provide the sense of touch, surface temperature, and pain[9]. Furthermore, it regulates moisture by preventing dehydration and loss of body nutrients[10].

The skin has a thermoregulatory control system comprised of four main mechanisms: sweating, shivering, vasoconstriction, and vasodilatation. This combination can maintain body core temperature within a very small range[11].

Thus, all these functions are combined to promote the maintenance of homeostasis of the body.

1.1.2. Structure

The skin is a multi-layered structure comprising layers that differ in their composition and structure, known as the epidermis, dermis, and hypodermis.

Epidermis

The epidermis is the most superficial layer of the skin and is itself divided into several layers starting with the top layer, the *SC* proceeding downwards through the prickle and the granular layers, to the basal layer or *stratum basale*, just above the dermis[12]. The epidermis is primarily formed by keratinocytes, squamous cells that originate in the *stratum basale*. These ectoderm-derived cells undergo terminal maturation, as they migrate from the basal layer of the epidermis towards the *stratum corneum*, at which they transform into corneocytes[13]. Melanocytes and Langerhans cells are two other important cell types in the epidermis, as the former confers protection against UV light and gives the skin its color, and the latter plays a key role on the immune barrier imposed by the skin[12].

The *stratum corneum*, skin's outermost barrier, is the well-recognized interface with the outside world that acts as a strong shield, in such a way that it counteracts unwanted penetration of materials and invasion of microorganisms, but also, prevents desiccation caused by excessive loss of water from the body[14,15]. In terms of the structural components, the *SC* is essentially composed of dead cells known as corneocytes, stacked up to 18-20 layers, depending on the anatomical location in the body, interconnected by corneodesmosomes and surrounded by a specialized lipid matrix that fills the tortuous pathway between the tight corneocytes. All of these components are crucial to the SC barrier function, from the very compact structure of corneocytes itself to the adjoining lipids, such as ceramides, cholesterol, and free fatty acids, responsible for providing a physical and permeability barrier, respectively[12,15]. Andrews *et al*. observed that removal of the *SC* drastically increased permeability, emphasizing, even more, the need to focus on enhancing the permeation through this layer to increase transdermal and topical drug delivery[16]. This prompted a further investigation on physical and chemical means of enhancing penetration of poorly absorbed drugs through the *SC*. Physical methods, such as iontophoresis, electroporation, sonoporation, and microneedle-enhanced delivery systems, are used to circumvent the *SC* and generically share a common goal: to disrupt *SC* structure and create holes big enough for molecules to permeate[17,18]. Nonetheless, the most convenient and common technique is the use of pharmacologically inactive compounds (chemical enhancers, CEs), also known as special formulation additives, which improve solubility within the *SC* and increase lipid fluidity of the intracellular lipids[19]. CEs diffuse into the skin and interact with *SC* components, being that penetration abilities of CEs change due to different interactions with drug or skin[19,20]. This

leads to an increase of the drug's diffusion coefficient and ultimately, a rise in the permeation rate through the corneocytes[20]. Numerous compounds have been studied for penetration enhancing activity, including sulphoxides, azones, pyrrolidones, alcohols and alkanols, glycols, surfactants, terpenes, and natural oils[21,22].

Dermis

Reinforcing the epidermis is the dermis, a connective tissue layer overlying the hypodermis, which accommodates the neural, vascular, lymphatic, and adnexa of the skin. It is described as being divided into two layers: a superficial papillary zone, lying deep to the epidermis, comprising relatively thin collagen fibers, and a much thicker reticular dermis zone composed of dense connective tissue that constitutes the bulk of the dermis[23]. The predominant cell types of the dermis are fibroblasts, responsible for the production of collagen fibers, and structural proteoglycan and elastin which embed macrophages and immune-competent mast cells[24]. Collagen protein is the principal component of the dermis, specifically, type I and type III collagen, which maintains skin strength and toughness[25]. Whereas proteoglycans support the hydration and viscosity, elastin enhances the deformability of this layer[26,27]. The dermis houses other skin components within these components and fibrous tissue such as blood and lymphatic vessels, nerve endings, hair follicles, and sweat glands. Albeit the thickness of the dermis varies according to the body part in question, it is a thicker layer than the epidermis, averaging from 0.6 mm to 3 mm[24].

Hypodermis

Lying beneath the dermis is the innermost fascia of the integumentary system in vertebrates, commonly known as the hypodermis or subcutaneous tissue[28]. The hypodermis is primarily composed of lipocytes, arranged into adipose lobules with interconnecting collagen and elastin fibers. Bundles of fibrous bands originating from the dermis and extending into the subcutaneous tissue strengthen the connection between these two compartments and anchor the skin to the underlying fascia and skeletal muscle. Hypodermis harbors along with some skin appendages like the hair follicles, sensory neurons, and blood vessels. Its primary functions are energy storage, endocrine regulation, protection against physical shock, and heat insulation[1,29].

1.2. Topical Delivery

The route of administration of a drug directly affects both the rate and the extent of bioavailability, which determines both the start and the duration of the pharmacological effect[30]. In nanotherapeutic studies, it is very important to choose the ideal route of

administration of a certain drug, bearing in mind that it may have an impact on its distribution, permeability, and effectiveness due to the variability in shape, size, and surface charge of nanoparticles[31].

Over the years, numerous successful bioactive compounds have been delivered across the skin to achieve controlled or prolonged drug delivery[32]. The administration of drugs across the skin is oftentimes seen as an alternative to the oral route, which faces substantial challenges regarding the irregular absorption in the gastrointestinal (GI) tract and low bioavailability for drugs with short plasma half-life times and liver first-pass metabolism[33]. Topical drug administration is the term utilized for application of the drug primarily to controlled areas of skin to get a localized effect, that is not intended for systemic distribution[34].

Topical drug delivery is a non-invasive, painless, and convenient way of delivering a drug, for therapeutic management or dermatological purposes. This administration route across the skin can offer many advantages, such as improved patient compliance, circumvention of liver first-pass metabolism, reduced side effects associated with peaks and troughs in drug plasma concentration, ease of dose termination when adverse effects occur, sustained drug release, and high local concentration of the drug rather than systemic levels, thus, providing a local effect[35,36].

1.2.1. Topical Versus Transdermal Drug Delivery: Understanding Differences

Generally, the terms topical and transdermal are used synonymously, but there is a major distinction between them – Figure 1.

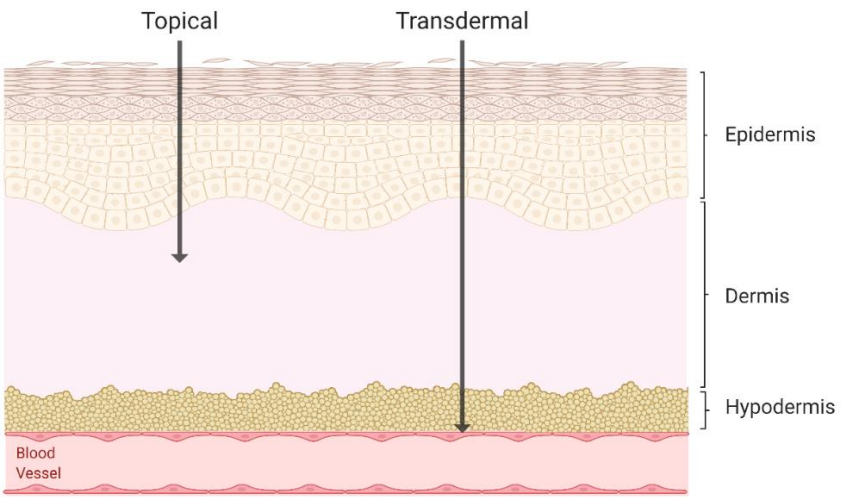


Figure 1 - Topical versus transdermal delivery across the skin layers.

As mentioned above, a topical administrated drug sits relatively a-top the skin, with limited penetration through the upper layers. On the other hand, a transdermal administrated drug can penetrate through deeper layers of the skin, reaching the bloodstream for a broader range of benefit[14].

1.2.2. Drug permeation pathways in the skin

The routes of permeation of the drug across the skin are broadly classified as the transcellular route (diffusion across corneocytes); the intercellular route (diffusion across the lipid matrix); and the shunt pathway or appendageal route (diffusion into the sweat gland, hair follicles, and sebaceous gland)[37] – Figure 2.

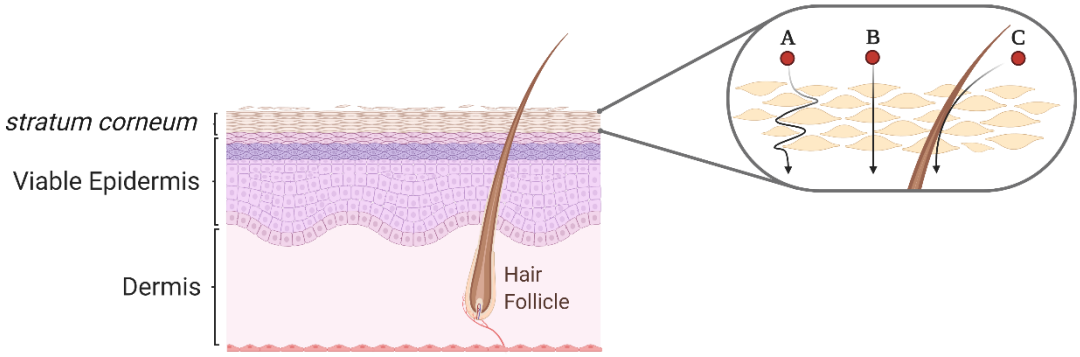


Figure 2 - Permeation pathways in the skin. (A) Intercellular route; (B) Transcellular route; (C) Appendageal route.

The transcellular route involves the passage through the cytoplasm of corneocytes, partitioning into the cellular membranes and intercellular lamellar lipid bilayers to deeper skin layers[38]. Therefore, drug encounters both hydrophilic and lipophilic regions, making this route very resistant to drug permeation[37,39]. Nonetheless, this drug permeation route tends to favor small hydrophilic molecules, since the keratin-filled corneocytes have an intracellular matrix that is relatively hydrated and, thus, polar in nature[40,41]. The intercellular route has been considered as the principal penetration pathway of drug molecules, which implies the navigation through the tortuous path within the extracellular matrix, along with the lipid lamellar, without partitioning into the cells[38,41]. Small hydrophobic drugs generally favor the intercellular route[37,39,42].

In the appendageal pathway, also known as the shunting route, permeant molecules travel through sweat glands, apocrine glands, and hair follicles with its associated sebaceous glands,

circumventing the *stratum corneum*[43]. This route's contribution for drug permeation into the skin is estimated to be small since the surface occupied by the appendages is only about 0.1% of the skin[37].

1.3. Factors affecting drug permeation

1.3.1. Physiological properties of the skin

Skin is a diverse tissue whose physiology varies considerably around the body and influence the delivery of the active into and through the skin.

Skin condition

Because the *SC* is the greatest barrier to drug permeability, any disease or abrasion that affects the continuity of the *SC*, its composition, and lipid organization, can lead to physiological changes[44]. These changes may encompass an increase in vasodilatation, which directly enhances the permeability of the skin[45].

Common inflammatory skin disorders such as atopic dermatitis and psoriasis negatively impact cutaneous permeability barrier function[46,47]. Skin burns and mechanical damages, such as cuts and abrasions, also affect the integrity and the barrier function of SC, leading to an increase in the rate of absorption[48,49]. This being said, the state of the skin (normal, abraded, and diseased) greatly influences the permeation of a drug across the layers.

Skin age

As the skin ages, it undergoes significant age-associated biological and biophysical changes within, which lead to altered drug permeability[50]. These notorious changes may include alterations in blood pressure, skin thickness, pH, hair and pore density, and the content and structure of proteins, glycosaminoglycans (GAGs), water, and lipids[51]. According to Donnelly and Singh, the permeability of drugs is higher in infants than in the elderly, since the *SC* is not fully developed and the water content is higher[48].

Race

Although there is no difference in skin penetration between different races, i.e., African, Asian, and European, it has been proven that darker pigmented skin types have a better barrier

that leads to the *SC* recovering slightly faster after perturbation than races containing a light-pigmented skin[48].

Skin temperature

Temperature impacts drug penetration through the skin by affecting the blood flow and increasing the metabolism in the skin. The effect of temperature can be seen as directly proportional, implying that when the temperature increases, the barrier permeability increases, and when the temperature decreases, the barrier permeability decreases. Passive transport through the skin is temperature-dependent and is illustrated by the Stokes-Einstein equation[52]:

$$D = \frac{k_B T}{6\pi\eta r} \qquad (1)$$

According to the Stokes-Einstein equation (Eq. 1), the diffusivity D (cm^2/sec) is directly proportional to the absolute temperature T (K) and Boltzmann constant K_B (cm^2*g/s^2*K) but inversely proportional to the viscosity of the media (g/cm*sec) and the hydrodynamic radius r (cm) of the molecules.

Skin hydration and occlusion

In human healthy skin, the *stratum corneum* typically contains water to an extent of 10 – 20% and provides a relatively efficient barrier against percutaneous absorption of exogenous substances[53].

Skin hydration leads to many changes regarding *SC*'s ultrastructure due to the increasing presence of water, swelling corneocytes, and possibly altered the intercellular lipid phase organization[54,55]. Additionally, it also affects the skin's rheological properties, as the skin becomes more elastic, causing an increase in the rate of penetration of most molecules[48]. In line with Donnelly and Singh, this can be explained by the *SC* diffusion coefficient, since it increases with a rise in water content, resulting in hydration and enhanced absorption through the skin.

Occlusion refers to covering the skin with impermeable or semipermeable materials, such as gloves, textiles, films, or even certain topical vehicles if they contain fats or some polymer oils. Skin occlusion obstructs the normal ventilation of the skin surface and causes the entrapment of water which would normally be lost to the surrounding. These events can

produce profound changes, mainly in *SC* hydration status and rise in temperature and ultimately, in barrier permeability. Thereby, this phenomenon enhances the percutaneous absorption of topically applied drugs and applied chemicals, and also favors the penetration of antigens and microorganisms[54,56].

1.3.2. Physicochemical properties of the drug

For an active molecule to cross the skin barrier at an acceptable rate, the physicochemical properties must be brought into consideration[57]. The measure of mobility of an active through environments, such as biological barriers, is known as the diffusion coefficient[52]. This physicochemical parameter affects the drug's bioavailability and biodistribution and is dependent on molecular size, solubility, ionisation, and the partition coefficient of the molecule.

Molecular Size

As can be seen in Eq.1, the diffusivity (D) within the *SC* is inversely proportional to the size of the permeant, and hence, a low molecular weight is desirable. This inverse relationship between permeant size and skin permeation has been reported[58]. As a general rule, the ideal size for a molecule penetrating intact *SC* should be less than 500-600 Da, when D tends to be high[59].

Solubility

The solubility of a drug is one of the most limiting physicochemical parameters, as it will greatly influence the diffusion of the active agent through the *SC*. Permeation of a molecule applied to the skin is favored if this molecule has a biphasic solubility, being both lipid and aqueous soluble, rather than a monophasic solubility. If a substance is too lipophilic, it will accumulate and remain in the layers of the *SC*, while being too hydrophilic will influence the penetration, leading to diminutive diffusion through the main barrier of the skin[60]. Besides possessing an adequate lipid solubility, due to the *SC* lipid nature, the layers beneath it dictate that molecules should also embody some hydrophilic properties to pass through them and hence, present a reasonable aqueous solubility (> 1 mg/mL)[29,59]. At last, a low melting point is also a good characteristic, since it correlates with good solubility of the drug in the intercellular *SC* lipid domain[59].

Solubility is a fundamental property that has to be evaluated in the early stages of drug discovery.

Ionisation

The absorption of a drug through the skin is inversely dependent on its degree of ionisation, and hence it is a determining factor for the successful delivery of a drug by both passive and assisted delivery mechanisms. Since the nature of the *stratum corneum* is predominately lipophilic and the particle needs to move through a largely lipophilic pathway, the ionized form of the molecule is less likely to penetrate the skin than the unionized form[48,61]. Ionized molecules are usually unable to penetrate lipid cell membranes because they are hydrophilic and poorly lipid-soluble, whereas unionized molecules are usually more lipid-soluble and can diffuse across cell membranes[62].

Partition Coefficient

The partition coefficient is a measure of the lipophilic-hydrophilic balance of a drug and an indication of its ability to cross the biological barriers, as it describes how an active is distributed and partitioned between two immiscible phases in the skin, the organic and aqueous layers at equilibrium[63]. Simplistically, a higher partition coefficient represents a more lipophilic molecule, and hence, is usually associated with an increase in permeation through the lipid domains of the *SC*[48]. For a molecule to penetrate intact *SC*, the optimal octanol-water partition coefficient value (log P) should be between 1 and 3. Drugs with log P values below 1 are too hydrophilic and have difficulties diffusing through the *SC*. In opposition, the ones with a log P value greater than 3, are too hydrophobic and may be retained in the lipid domains of the *SC*, but also, present low permeation rates in the aqueous environment of the viable epidermis, which can affect therapies whose purpose is a systemic effect through the bloodstream[59]. Thereby, taking into account that a log P value of 0 means that the compound is equally partitioned between the lipid and aqueous phase, this ideal range of log P values for effective drug penetration implies that the latter should present an adequate lipid phase affinity, but still possess some aqueous affinity properties[64].

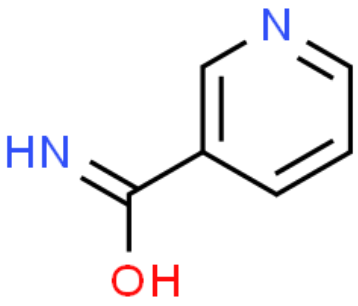
1.4. Niacinamide

Niacinamide, chemically known as pyridine-3-carboxamide, is an amide form of vitamin B3, and a water-soluble molecule with a wide range of mechanisms of action, that have long been described in the literature[65,66]. This vitamin is not naturally stored in the body, but it can be obtained by the dietary intake of vitamin B3 and tryptophan. Vitamin B3 can be found in a wide variety of food including meats, seafood, fruits, legumes, dairy products, and grain products[67]. NIA is a precursor to energy co-factors *in vivo*, such as nicotinamide adenine dinucleotide (NAD)

and nicotinamide adenine dinucleotide phosphate (NADP). Whilst NADP is produced from NAD by phosphorylation, one of the ways that the biosynthesis of NAD occurs is from NIA, through a two-step process via the salvage pathway[68,69]. Since these co-enzymes are involved in many cellular oxidation-reduction reactions and thus can potentially influence many skin mechanisms, the intake of NIA is a very important aspect[70]. Both a deficiency and an excessive intake of NIA can lead to adverse side effects. Whereas the deficiency of NIA can cause pellagra, a dermatological condition, the intake level per day exceeding 35 mg of NIA in adults (19 years of age or older) may cause complications[67,71].

As discussed in the last topic, the physicochemical properties of a drug are a determining aspect for the permeation of the active through the skin. The physicochemical characteristics of NIA are given in Table 1.

Table 1 - Physicochemical properties of NIA

Chemical name	3-Pyridinecarboxamide; nicotinic acid amide
Generic name	NIA; nicotinamide; vitamin B3; vitamin PP
pKa	3.35
Molecular Size	122.1 Da
Molecular weight	122.12 g/mol
Melting point	128 - 131 °C
Appearance	White crystal powder
Taste	Bitter and salty
Odor	Odorless
pH	pH 3.0 – 3.5
Log P	- 0.37
Solubility	212.95 mg/mL
Density	1.44 g/cm^3
Chemical structure	

Information obtained from PubChem database[72]

In terms of molecular size, NIA is considered a small molecule with a molecular size of 122.1 Da, and therefore, could be absorbed well through the skin. Nevertheless, this active compound has at least three physicochemical properties that defy its penetration across the skin, namely

the solubility, the partition coefficient, and the pKa. NIA has an aqueous solubility of 212.95 mg/mL, meaning that it is extremely soluble in water and thus, the permeability through the lipophilic *stratum corneum* may be a problem. Also, the low partition coefficient represented by a log P value of – 0.37 demonstrates the low permeability of the membrane to this substance, since it expresses the higher solubility of NIA towards the water phase than in the lipid phase. In addition, this molecule has a pKa of 3.35, which implies that this substance is fully ionized at a pH of 7.4, making it difficult for the asset to pass through the *SC*, as discussed previously in this section[73].

Several recent studies demonstrated that systemic level NIA has shown promise as a well-tolerated and cost-effective agent against skin cancer prevention and therapy[74,75]. When applying the active topically, NIA could be suitable for use in disorders such as hyperpigmentation, melasma rosacea, acne, atopic dermatitis, and in abrogating features of ageing[76,77].

1.5. Ageing

Everything began with the free radical theory, one of the important theories for ageing, which was proposed by Denham Harman in the 1950s, wherein the generation of free radicals results in damage to the connective tissues and cell constituents, including DNA and RNA[78]. This was later extended to include mitochondrial production of reactive oxygen species (ROS), and oxidative stress caused by some degenerative diseases, like Alzheimer's disease[79].

In healthy skin, practically all types of skin cells are continuously producing free radicals, such as ROS, derived from cellular respiration, metabolic processes, and external aggressions[80]. Cellular homeostasis is carefully maintained by an elaborate network of endogenous antioxidants that neutralize the free radicals without becoming destabilized themselves, thus attenuating the damaging effects of ROS. The imbalance between free radicals and endogenous antioxidants arises in a phenomenon called oxidative stress[79,81]. This phenomenon affects the skin's biological molecules and induces changes that accumulate over time. The ageing process results from this accumulation of oxidative damage that occurs in cells and tissues, and these counter-attack mechanisms are no longer present in the amount necessary to combat oxidative stress. In the case of the skin, its ageing can be reflected in the form of wrinkles, pigmentation changes and a more fragile appearance due to the atrophy of the epidermis and dermis[82].

Skin ageing has both intrinsic and extrinsic causes, and although these types differ, the effect is synergistic and leads to an aged look to the skin. Whereas intrinsic ageing occurs as a natural consequence of ageing and is genetically determined, extrinsic factors are, to varying degrees, controllable and include exposure to UV radiation, pollution or nicotine, repetitive mechanical

movements, and diverse lifestyle components such as diet, sleeping position, and overall health[83].

Also, the ageing of the skin causes changes in its composition. Intrinsic and extrinsic factors lead to a reduction in cell proliferation, making the epidermis thinner and decreasing its contact with the dermis, resulting in a reduction of nutrients that reach the most superficial layers of the skin. Cells such as keratinocytes, fibroblasts, and melanocytes become senescent and there is a decrease in the amounts of elastic fibers and collagen, reducing the elasticity of the skin, and oligosaccharides, reducing the hydration of the skin[84].

1.5.1. The treatment of ageing with NIA

Several agents can be used to fight or delay the aging of the skin, such as growth factors, retinoids, acids of natural origin and derivatives, protectors from solar radiation, and exogenous antioxidants[85]. According to Ramos-e-Silva *et al.*, antioxidants are mainly free radical scavengers that lessen the cellular damage caused by oxidative stress and offer protection against photodamage and skin cancer. These antioxidants include alpha-lipoic acid, L-ascorbic acid, α-tocopherol, ubiquinone, and NIA, the latter being a powerful and well-tolerated one[86].

NIA shows a stabilizing effect on epidermal barrier function causing a significant reduction in the transepidermal water loss[86]. It also acts as an effective skin lightening compound that decreases hyperpigmentation by inhibiting melanosome transfer from melanocytes to keratinocytes[87]. It is known that one of the best strategies for preventing and reversing skin wrinkles and fine lines is to inhibit oxidants by using antioxidants like NIA, which delay the aging process by countering the breakdown of collagen and elastin fibers in the skin[88]. Also, vitamin B3 increases the biosynthesis of ceramides, as well as other *SC* lipids, that are reduced in aged skin, and improves the moisture content of the horny layer[69,89].

1.6. Drug Delivery Systems

The topical delivery of NIA is a problem since its physicochemical properties are not ideal. That being said, there is a need to use a delivery system to mask NIA's physicochemical properties that hinder its penetration through the skin. In the present study, the main focus will be to evaluate hydrogels and transethosomes applicability for NIA skin delivery.

1.6.1. Hydrogels

Hydrogels are three-dimensional (3D) crosslinked polymer networks, which can absorb and retain a large amount of water due to their hydrophilic groups[90]. Hydrogels have become highly relevant for a wide range of biomedical applications, especially in drug delivery and tissue/organ repair fields, due to their unique and tunable properties in terms of their porosities, mechanics, interfacial dynamics, and biological responses, as well as their versatile fabrication methods[91]. Hydrogels can be classified based on cross-linking and are divided into two categories: physically crosslinked or self-assembled hydrogels and chemically crosslinked hydrogels. Whilst the former can undergo a transition from liquid to a gel in response to a change in environmental conditions such as temperature, ionic concentration, and pH, the latter relies on covalent bonds that exist between different polymer chains, that lead to increased hydrogel's stability, mechanical integrity, and degradation resistance[92]. Besides, hydrogels can be further classified in many different ways, based on their sources (natural or synthetic hydrogel), polymeric compositions (homo-polymer, co-polymer, and multi-polymer hydrogels), physical structure (amorphous, semi-crystalline, and crystalline hydrogels), ionic charges on the bound groups (nonionic, cationic, anionic, amphoteric and zwitterionic hydrogels) and release controllers (time-controlled hydrogels and stimuli-induced or smart hydrogels)[90,93]. Compared with other types of biomaterials, hydrogels have numerous advantages in drug delivery including increased biocompatibility, tunable biodegradability, low toxicity, proper mechanical strength, and a porous structure adequate to incorporate the active agents[94].

Carrageenan hydrogels

Polysaccharides have attracted much interest due to their inherently desirable biocompatibility and interaction with biological systems, being widely proposed as carriers for drug delivery systems[95]. Carrageenan is a seaweed-based polysaccharide that can be conventionally categorized into six basic forms, depending on the number and the position of sulphate groups, source of extraction and solubility: Kappa (κ)-, Iota (ι)-, Lambda (λ)-, Mu (μ)-, Nu (ν)- and Theta (θ)-CRG. However, k- CRG is one of the most commercialized and the most suitable forms for drug delivery and tissue engineering purposes due to its viscoelastic and gelling properties[90,96]. κ-CRG is a natural-origin polymer that closely mimics the glycosaminoglycan structure, one of the most important constituents of native tissues extracellular matrix, as it comprises repeating units of (1,3)-D-glucopyranose and (1,4)-3,6-anhidro-α-D-galactopyranose with one sulfate group, per disaccharide unit[97,98]. κ-CRG is a non-toxic, hydrophilic, biodegradable, and anionic molecule, with great gelling properties, as in aqueous solutions and in the presence of several cations, forms on cooling, thermoreversible gels[97,99]. According to Liu *et al.*, the gelation

process of κ-CRG hydrogels is dependent on the temperature, κ-CRG concentration and is achieved by two steps[100]. It is widely used in cosmetic applications in hydrogel form, acting as a moisturizer, conditioning agent, and a retainer of water onto skin and hair[101].

1.6.2. Nanocarriers

The use of a nanosized vehicle system to deliver beneficial compounds to the skin aims to[85]:

- improve the stability of drug molecules, protecting them from degradation;

- increase its penetration into the layers of the skin, especially in the epidermis, so that they reach their target;

- allow a more controlled and prolonged release of the active substance at the target site, amplifying its effect;

- minimize side effects, such as skin irritation, by encapsulating these substances;

- reduce costs and a more efficient formulation allows reducing the waste of normally expensive materials.

The use of nanocarriers can allow a controlled and prolonged release and a variety of them can be used in skin applications, from liposomes, niosomes, transferosomes, ethosomes, nanoemulsions, solid lipid nanoparticles (SLNs), nanostructured lipid carriers (NLCs), among others[85].

Transethosomes

Taking into account everything that has already been said about the physicochemical properties of the compounds and the barriers that must be overcome to achieve a good topical action, the drug delivery vehicle chosen for this study is the transethosome. This type of nanoparticle is found in the class of liposomes but can be considered as an improvement of the latter, regarding skin delivery. Transethosomes appeared in 2012, merging the advantages of classic ethosomes (which, due to the presence of ethanol, are already considered better than liposomes for skin delivery) and transferosomes (also called deformable liposomes, due to the presence of edge activators)[102–104] – Figure 3. In this way, the transethosomes can become deformable and also penetrate well into the skin[104]. Since transethosomes contain both hydrophobic and hydrophilic entities, they can enclose drug molecules with a wide range of solubility[105].

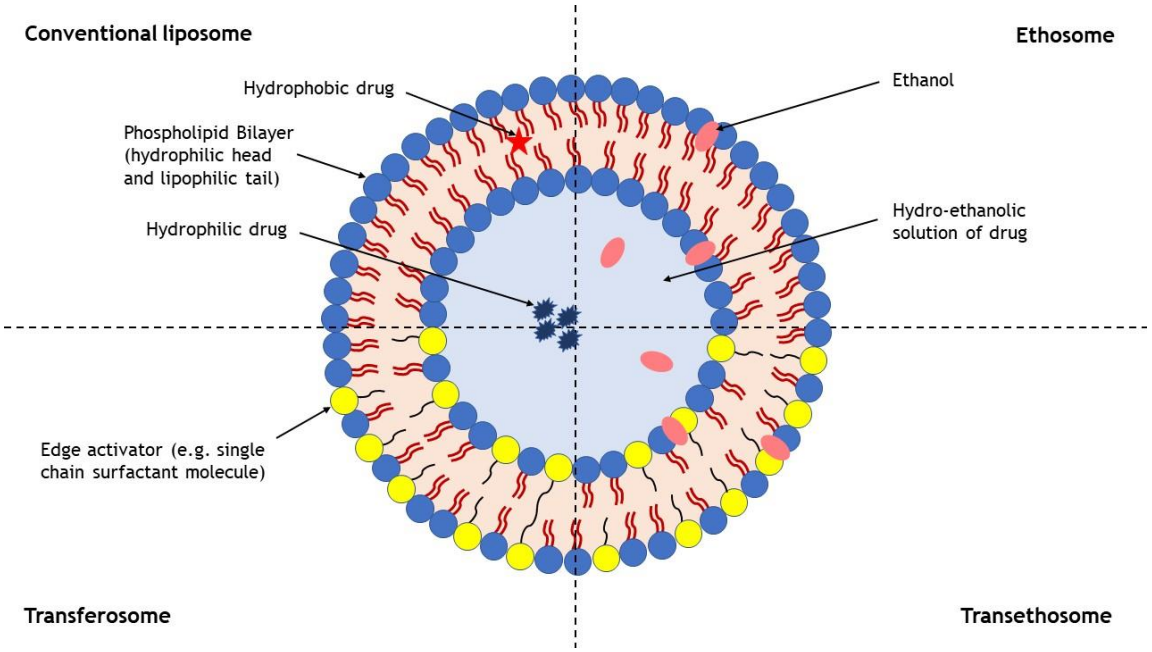


Figure 3 - Representative image of the structural composition of conventional liposomes, ethosomes, transferosomes and transethosomes. Adapted from[36].

These systems are essentially constituted by: phospholipids, such as conventional liposomes; ethanol in high concentration (up to 40%), a characteristic they acquired from ethosomes; edge activators (like tween 20, tween 60, tween 80, span 60, span 65, span 80, sodium cholate or sodium deoxycholate) or permeation enhancers (PEs) (e.g. oleic acid), a characteristic that comes from transferosomes; and water[102,106].

One of the components that distinguish this type of nanoparticle from traditional liposomes is the presence of ethanol, which is a crucial component of transethosomes, as it acts as an efficient penetration enhancer. Ethanol interacts with the polar heads of the phospholipids, exerting a fluidizing effect on the lipid membrane, which will disturb biological membranes. This disturbance will alter the organization of the *stratum corneum* lipids, increasing the penetration of this nanosystem through the skin[107]. Also, the presence of ethanol gives a negative charge to the nanocarrier, making it smaller in size and more stable over time[108].

In addition to ethanol, edge activators or penetration enhancers are also important constituents of transethosomes, as they function as a key factor for ultra-deformability to this liposomal type of vehicle. Edge activators are membrane softening agents, that are capable of changing the membrane's flexibility and enhance permeability across the skin[109].

Some delivery systems have already been developed for the application of niacinamide to the skin:

- Lee *et al.*, studied the skin permeability and anti-melanogenesis activity of NIA, by incorporating it into flexible liposomes with the edge activator dipotassium glycyrrhizate[110]. The skin permeability of NIA in these flexible liposomes was significantly higher than that of conventional liposomes.

- Offerta *et al.*, evaluated different strategies to optimize the percutaneous absorption of NIA and soy phytosterols by making use of solid lipid nanoparticles and penetration enhancers, such as hydrogenated lecithin[65]; There was an increase in percutaneous absorption of both active.

- Shin *et al.*, developed novel microneedle-like particles whose needles would disrupt the skin during the rubbing process to enhance NIA penetration[111]. This study demonstrated that these particles were capable of disrupting the skin layer to increase the skin permeability of NIA.

It is worth mentioning that the delivery systems developed in this study are a novel approach for the topical application of niacinamide, given the selected systems, hydrogel and transethosomes as well as the incorporation of a CE – the jojoba oil.

2. Motivation

This study aims to analyze the topical skin delivery of niacinamide by formulating and optimizing two drug delivery systems: hydrogels and transethosomes. This comparative study will allow not only to evaluate the effectiveness of each system in enhancing the permeation of this compound through the skin, in an attempt to determine which is the ideal but also to obtain in-depth knowledge of the system's production and characterization techniques.

To address this challenge, specific aims of the work described in this thesis focus on:

1. Validation and implementation of a high-performance liquid chromatography (HPLC) method for the quantification of niacinamide.
2. Design, optimization and characterization of carrageenan-polyvinylpyrrolidone based hydrogels to deliver niacinamide.
    a. Characterization of the delivery system, which includes measuring pH, analyzing swelling properties, detecting functional groups and characterizing covalent bonding information through Fourier-transform infrared spectroscopy and analysis of the surface per scanning electron microscopy (SEM).
3. Formulation, optimization and characterization of transethosomes containing niacinamide.
    a. Characterization of this vesicle system by performing particle size (PS), polydispersity index (PDI), zeta potential (ZP), bioactive agent content, and storage stability measurements, as well as, identifying chemical bonds through FTIR and morphology per transmission electron microscopy (TEM).
4. Formulation of the optimized carrageenan-polyvinylpyrrolidone based hydrogel containing the transethosomes, for a more in-depth knowledge of this comparative study.
5. Determination of the skin permeation profile of the developed delivery systems using pig ear skin in Franz diffusion cells, to determine the concentration of niacinamide being delivered through and into the skin.

3. Materials and Methods

3.1. Materials and Instrumentation

Niacinamide, κ-CRG, 1-ethyl-3-(3-dimethylaminopropyl) carbodiimide hydrochloride (EDC), tripolyphosphate (TPP), polyvinylpyrrolidone, polyvinyl alcohol (PVA), JO, Tween-80, oleic acid, 4-(2-hydroxyethyl) -1-piperazineethanesulfonic acid (HEPES) powder, chloroform, trypsin and phosphate-buffered saline (PBS) weyre supplied by Sigma-Aldrich (St Louis, MO, USA). Egg yolk phosphatidylcholine (EPC) was acquired from Avanti polar lipids (Alabaster, AP, USA). Ethanol absolute (≥ 99,8%) and methanol (≥ 99,8%, HPLC grade) was obtained from Fisher Chemical (Thermo Fisher Scientific, Loughborough, UK). Double-deionized water was provided by a double-deionized water system (Arium Pro, Sartorius AG, Göttingen, Germany). The porcine ears were acquired in a local slaughterhouse located in Porto, Portugal. Reagents were weighted in a Kern ACJ/ACS 80-4 (Kern & Sohn; Balingen, Germany) digital analytical balance and the pH measurements were achieved using a Crison pH meter GLP 22 with a Crison 52-02 tip (Crison, Barcelona, Spain).

All non-referenced illustrations in this thesis were created in BioRender's web software.

3.2. Preparation and Optimization of Drug Delivery Systems

3.2.1. Preparation of carrageenan-based hydrogels

κ-CRG was the base polymer used in the formulation of all hydrogel matrices developed in this study, for controlled niacinamide delivery. The hydrogels were prepared by dissolving the polymer powder in double-deionized water and heating at 60 - 70ºC while stirring in a magnetic stirring plate (IKA-Werke, Staufen, Germany), for 30 min or until a clear solution was obtained. The mixture was allowed to cool slowly during 24 h, until the gelation was complete. In hydrogels containing niacinamide, the active agent was added 10 min before the cooling step. The co-polymer and/or crosslinked hydrogels followed this same procedure, except that before mixing in double-deionized water, they were weighted together with κ-CRG.

Visual appearance and texture were evaluated in 24 h and the pH of all hydrogels was measured using a Crison pH meter GLP 22 with a Crison 52-02 tip (Crison, Barcelona, Spain).

3.2.2. Optimization of carrageenan-based hydrogels

In terms of hydrogel optimization, two synthetic polymers were tested. These formulations (F) were prepared by the previously described method, and their composition is shown in Table 2.

Table 2 - Optimized carrageenan hydrogels with different compositions

Ingredient % (w/v)	F1	F2
CRG	1	1
PVP	—	1
PVA	1	—

To study the effect of a permeation enhancer on the ability of CRG hydrogels to permeate niacinamide through the skin, jojoba oil was selected and added to the CRG-PVP mix at the same time interval of both polymers. Four compositions with niacinamide 1% (w/w), in regard to the total polymer weight, were made and their composition is shown in Table 3.

Table 3 - The composition of four hydrogels with different JO percentages

Ingredient % (w/v)	Type A	Type B	Type C	Type D
CRG	1	1	1	1
PVP	1	1	1	1
JO	0	0.5	1	5

The formulations shown in Table 3 were used for the *in vitro* skin permeation studies, as described hereunder.

3.2.3. Preparation of transethosome formulations

Three types of transethosomes were prepared using different surface-active agents (SAAs): Tween-80, oleic acid, and jojoba oil. Their composition is shown in Table 4.

Table 4 - The composition of transethosomes

Ingredient (mg)	Type I	Type II	Type III
EPC	20	20	20
Tween-80	2	—	—
Oleic Acid	—	2	—
JO	—	—	2
Ethanol (µL)	600	600	600
Water (µL)	2400	2400	2400

Transethosomes containing NIA were prepared by the thin-film hydration method, illustrated in Figure 4. First, EPC and SAAs were weighed and dissolved in a mixture of methanol: chloroform (1:3, v/v), in a round bottom glass tube. By maintaining pressure under vacuum for 20 min, the organic phase was slowly evaporated at 40ºC using a rotary evaporator (Buchi Rotavapor R-200, Switzerland), till a thin clear film of lipid mixture was formed on the inner lines of round bottom tube. The film was hydrated with water and vortexed for 2 min. When necessary, the water bath at 45ºC was used to enhance the detachment of the thin film from the round bottom tube walls. Posteriorly, the specified volume of ethanol was added and the formulation was vortexed for 1 min. Then prepared dispersions were subjected to ultra-sonication using a probe sonicator (VCX130, Sonics and Material Vibra-Cell™ with a CV-18 probe; 115 Newtown CT, USA), for 5, 10 and 30 sec regarding Type I, II and III, respectively.

For the purpose of comparison in characterization techniques, both non-loaded and niacinamide-loaded transethosomes were prepared by the previously described method. The difference lays in the hydration step, as the film was hydrated with 2400 µL of double-deionized water in the non-loaded nanoparticles and hydrated with 2400 µL of a water solution containing 30 mg of niacinamide for loaded-transethosomes.

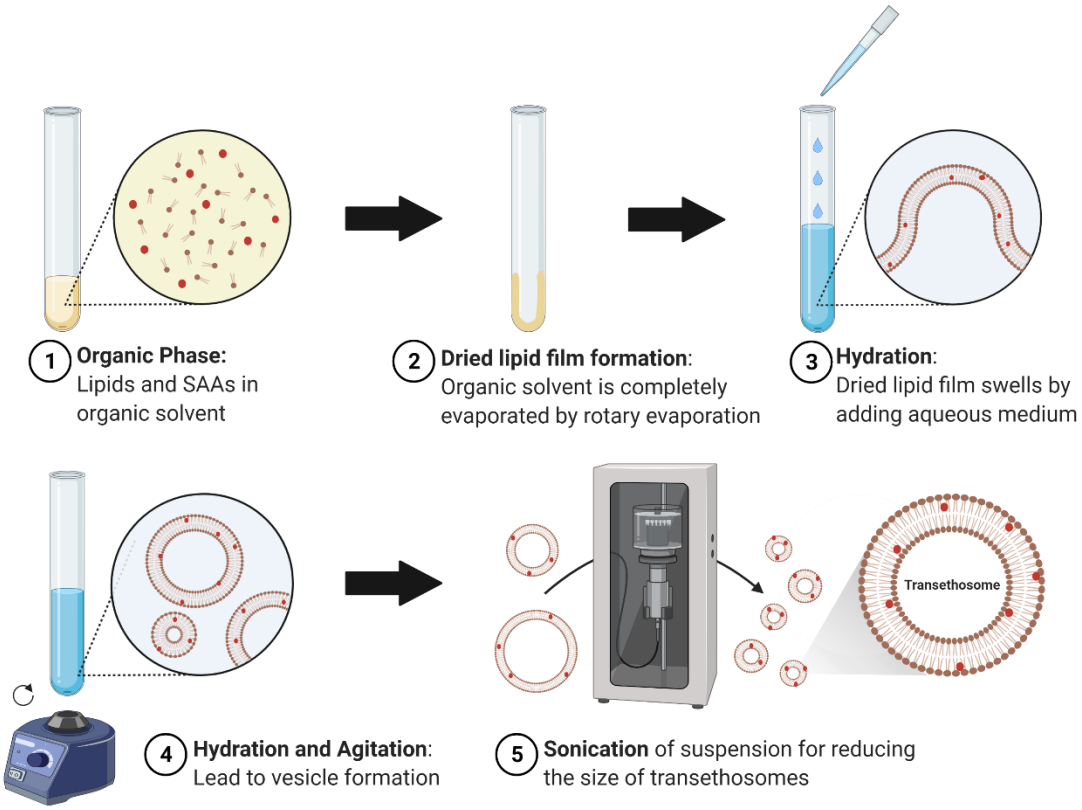


Figure 4 - Transethosome formulation via thin film method.

3.2.4. Transethosomes-loaded hydrogels

To study the permeation capacity of the two drug delivery systems together, transethosomes were incorporated into one of the optimized CRG-hydrogels and *in vitro* permeation studies were performed as well.

3.3. Characterization Techniques of Hydrogels and Transethosomes

3.3.1. Fourier-transform infrared spectroscopy evaluation

The hydrogels and TEs were analyzed using a FTIR Spectrophotometer (Frontier™, PerkinElmer; Santa Clara, CA, USA) equipped with an attenuated total reflectance (ATR) device and zinc selenite crystals, after freeze-drying. To do so, 3 g of each hydrogel and 2 mL of each formulation were placed into separate 15 mL falcons and kept overnight in a −80ºC freezer (Deep Freezer, GFL®, Burgwedel, Germany), to be further lyophilized in a freeze drier (LyoQuest –85 plus v.407, Telstar® Life Science Solutions, Terrassa, Spain) for 72 h, continuously kept at −80ºC and 0.40 mbar of pressure. The hydrogels, NIA-loaded transethosomes, as well as reference compounds, were placed directly on top of the ATR crystal for analysis at room temperature, after a background run with the ATR crystal alone to be considered as a negative control. Obtained spectra were a result of 32 combined scans recorded between 4000 and 600 cm^{-1}, with spectral resolution of 8 cm^{-1}. The spectra data of EPC and was obtained from literature[112].

3.3.2. Morphological analysis

Scanning electron microscopy

The morphology of freeze-dried hydrogels was analyzed by scanning electron microscopy (SEM) using a FEI Quanta 400 FEG ESEM/EDAX Pegasus X4M with an accelerating voltage of 10 kV. Hydrogels were fixed onto carbon-taped metal pins and coated with Au/Pd by sputtering for 45 s.

Transmission electron microscopy

The morphology of the NPs was observed by transmission electron microscopy (TEM, Jeol JEM-1400; JEOL, Ltd., Tokyo, Japan). In each measurement, one drop (ca. 10 µL) of each sample

was placed on a copper grid for 1 min. Then, 10 µL of 0.75% (w/v) uranyl acetate were added as contrast agent and left 30 sec in contact. The excess was removed with filter paper and the grid was exposed at the accelerating voltage of 60 kV for analysis and images capture.

3.3.3. Swelling assay

The swelling ratio (SR) of hydrogels was studied by measuring the mass weight after swollen at time points 1 h and 24 h. Three grams of all hydrogels were placed in 10 mL of swelling solvent, in an incubator shaker (ES-60E Incubator Shaker, Miulab, Hangzhou, Zhejiang, China) at 32 ºC and 125 rpm. Initially, the assay was performed in double-deionized water and later, other conditions were tested using solutions with different pH and/or salt concentrations. Samples were then carefully withdrawn, removing all free water, and then weighted. The SR (%) was calculated according to Eq.2.

$$SR = \frac{Weight\ wet - Weight\ dry}{Weight\ dry} \times 100\ \% \qquad (2)$$

3.3.4. Transethosomes vesicles size, polydispersity index and zeta potential

The PS, PDI and ZP of the transethosomes were determined using a ZetaPALS zeta potential analyzer (Brookhaven Instruments Corporation; Holtsville, NY, USA). Samples were first diluted in double-deionized water (1:10). In particle size measurements, six runs of 2 min were performed at room temperature for each assay. The zeta potential of the nanoformulations was determined using an electrode operating at a scattering angle of 90ºC at room temperature. For each assay, six runs of 10 cycles were performed.

3.3.5. Analytical method

NIA analysis was conducted using a HPLC equipped with a reversed-phase monolithic column (Chromolith® RP-18e, 100 mm × 4.6 mm i.d., Merck), connected to a Jasco (Easton, USA) HPLC system (pump PU-4180, autosampler AS-4050 and LC-Net II/ADC controller) coupled to a PDA detector (Jasco MD-4010, Start Wavelength = 200 nm, End Wavelength = 400 nm). The data processing was performed by ChromNAV 2.0 HPLC software (Easton, USA). The chromatogram was acquired at a wavelength of 263 nm, and the retention time of NIA was at 4.8 min. The mobile phase consisted of water: methanol (80:20). The injection volume was set to 20 µL, and the flow rate was 1 mL/min with the column temperature at 30ºC. Prior to use, the mobile

phase was degassed in an ultrasonic bath for 30 min. Validation of HPLC method was performed by evaluating linearity, range, accuracy, precision, lower limit of quantification (LOQ) and upper limit of detection (LOD) according to established guidelines[113,114]. To do so, calibration curves ranging from 1 – 30 µg/mL were prepared and analyzed in triplicate, comprising three independent experiments (n=3).

3.3.6. Determination of the entrapment efficiency and drug loading capacity

The ultrafiltration method was utilized for the estimation of entrapment efficiency and drug loading capacity of developed formulations, using an Allegra®X-15R centrifuge (Beckman Coulter, Pasadena, CA, USA). The amount of niacinamide entrapped in each formulation was determined by centrifuging 2 mL.

The niacinamide-loaded nanoformulations were diluted (1:20) with double-deionized water up to 2 mL, so the expected concentration of the active compound was within the calibration curve. The dilutions were placed in cleaned Amicon Ultra-4 Centrifugal Filter Units (Merck Millipore Ltd., Carrigtwohill, Co Cork, IRL) and centrifuged at 4500 rpm for approximately 30 min or until complete separation between the nanoparticles retained in the filter and the solvent phase corresponding to the supernatant. The supernatant representing the unentrapped niacinamide was rejected and the filter portion of the amicon tubes was put upside down inside a 50 mL falcon tube and centrifuged at 4500 rpm for 15 min, until the pellet was completely transferred. Following this, 200 µL of methanol were added to each formulation's pellet and vortexed for 1 min. Then, to match the ratio of the mobile phase used in the quantification method, 800 µL of water were added, and the amount of niacinamide in the supernatant was quantified using HPLC analysis, as previously described.

The encapsulation efficiency (EE) is defined as the percentage of drug incorporated into the lipid nanoparticles relative to the total drug added[115]. It specifies the percent of drug included in the particles and, indirectly the amount of free drug non-incorporated within the nanoparticle. The EE is calculated by the following formula:

$$EE\ (\%) = \frac{Total\ entrapped\ drug\ mass}{Total\ inicial\ drug\ mass} \times 100 \qquad (3)$$

The loading capacity (LC) is defined as the percentage of drug incorporated into the nanoparticles (NPs) relative to the total amount of NPs (lipid and SAA)[116]. The LC is calculated as following:

$$LC\ (\%) = \frac{Total\ entrapped\ drug\ mass}{Total\ nanoparticle\ mass\ (lipid + SAA)} \times 100 \qquad (4)$$

3.3.7. Stability studies

Optimum TEs were stored at 4ºC for 2 weeks. Samples were withdrawn each week and stability was evaluated by comparing the initial measurements with results obtained after storage. The EE%, LC%, PS, PDI, and ZP of the vesicles were measured as previously described.

3.4. *In Vitro* Permeation Studies

3.4.1. Skin Preparation

Pig ear skin was obtained from healthy animals at a local slaughterhouse. The skin was initially cleaned, and then hairs and subcutaneous fat tissue were removed. The full thickness membranes obtained were stored at −20ºC for no longer than two weeks before use. Before the experiments described below, the skin was allowed to thaw at room temperature and cut into circles of approximately 2.5 cm in diameter. No ethical approval needed.

3.4.2. *In vitro* skin diffusion studies

Skin permeation studies were performed using a Franz diffusion cell system (9 mm unjacketed Franz Diffusion Cell with 5 mL receptor, O-ring joint, clear glass, clamp, and stir-bar; PermeGear, Inc., Hellertown, PA, USA), as illustrated in Figure 5. The control sample in all experiments was free niacinamide dissolved in water at the same amount as in the formulation samples.

The prepared skin was placed in the Franz diffusion cells with the *stratum corneum* facing the donor compartment. The exposed skin surface area was 0.75 cm^2 and the receiver compartment volume was filled with 4.7 mL of HEPES buffer (to allow the establishment of physiological mimetic conditions and to sustain permeant solubilization), stirred and thermostated at 37 ± 1 ºC, during all experiments. On top of the skin surface in the donor compartment, a volume of 250 µL (50 µg of niacinamide) of each sample was placed, initiating the course of the experiment. At fixed timepoints 1, 3 and 6 h, samples of 1 mL were withdrawn from the receiver chambers, and replaced with the same volume of fresh medium.

Experiment conditions of *in vitro* permeation assays with TEs were replicated, the only exception lays in the fact that formulations had to be filtered before the experiments, in order to separate the loaded-transethosomes from the non-retained niacinamide in the formulation medium. This was achieved by the ultrafiltration method utilized for the determination of entrapment efficiency and drug loading capacity of developed formulations.

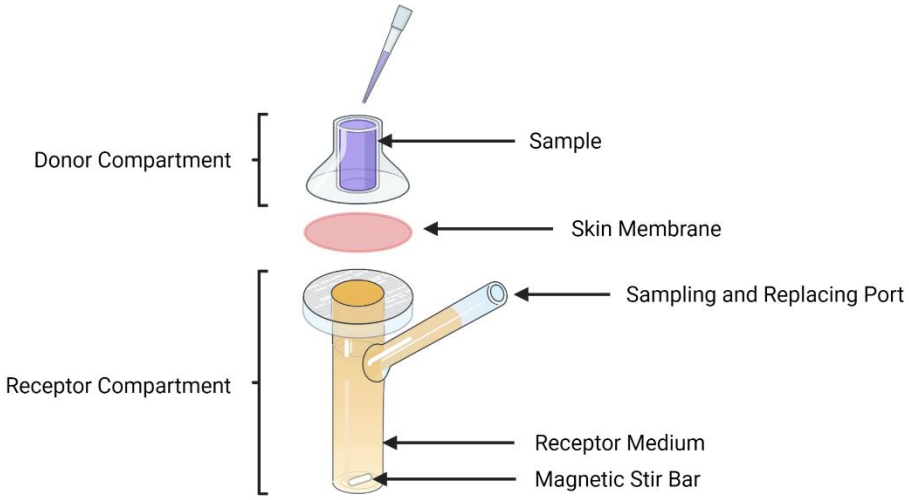


Figure 5 - Franz diffusion cell system. Adapted from[117].

Apparent permeability (P_{app}) was determined accordingly to the following equation:

$$P_{app} \quad (cm/s) = \frac{\sum m_a}{m_d \cdot A \cdot t} \tag{5}$$

The P_{app} was estimated by the ratio of the sum of the mass of NIA (m_a / g) permeated across the skin and the product of the initial mass in donor chamber (m_d / g), the diffusion area between cells in Franz diffusion system (0.63585 cm^2) and the time (time point 3 hours = 10800 s).

3.5. Statistical Analysis

Statistical analysis was performed using the GraphPad Prism Software (Version 6.01 for Windows; GraphPad Software Inc, San Diego, CA, USA). The two-way ANOVA analysis of variance was used to assess the differences between formulations.

4. Results and Discussion

4.1. Validation of HPLC method for Niacinamide

4.1.1. Purpose of validation

The purpose of this validation was to ensure the analytical method was accurate and precise in order to analyze niacinamide.

4.1.2. Chromatographic conditions

The chromatographic conditions for the validation of niacinamide are given in the table below.

Table 5 - Chromatographic conditions

Analytic instrument	Jasco (Easton, USA) HPLC system (pump PU-4180, autosampler AS-4050 and LC-Net II/ADC controller) coupled to a PDA detector (Jasco MD-4010, Start Wavelength = 200 nm, End Wavelength = 400 nm)
Column	Chromolith® RP-18e, 100 mm x 4.6 mm i.d., Merck
Mobile phase	Water: methanol (80:20)
Flow rate	1 mL/min
Injection volume	20 µL
Detection	UV at 263 nm
Retention time	4.8 min
Stop time	6.0 min
Solvent	Skin permeation media (24 h skin incubation with HEPES at pH 7.4 in a Franz diffusion system)

4.1.3. Validation parameters

Validation is where the performance characteristics of the procedure meet the requirements of the analytical applications. The performance characteristics used in the validation method were linearity, range, LOQ and LOD, accuracy, and precision[114].

4.1.4. Standard and sample preparations

For the standard preparation, 5 mg of niacinamide was accurately weighed and placed into a 50 mL volumetric flask to obtain a 0.1 mg/mL solution. The sample was made up to volume with buffer HEPES: methanol (80:20). From the standard preparation, dilutions were made with skin permeation media, at different concentrations ranging from 1 – 30 µg/mL. Calibration curves were prepared and analyzed in triplicate, comprising three independent experiments (n=3).

4.1.5. Linearity and range

Linearity of an analytical procedure is the ability to obtain test results that are proportional to the amount of the analyte in the sample. The range of an analytical procedure can be described as the interval between the upper and the lower concentration of the analyte in the sample, which shows the analyte has a suitable level of precision, accuracy and linearity[118]. The data can be described by the following linear equation:

$$y = ax + b \qquad (6)$$

Where y is the peak area, a is the slope, x is the concentration and b is the y-intercept[113].

The calibration curve is considered valid if it fulfills the following requirements:

- ✓ It is constructed based on at least 5 points;
- ✓ The concentration range differs on a 10-fold factor (at least);
- ✓ The relative standard deviation of the slope is lower than 5% ($S_a/a < 0.05$);
- ✓ The correlation coefficient (r) is greater than 0.995;
- ✓ The correlation coefficient (r^2) value must be ≥ 0.999, to ensure HPLC system stability.

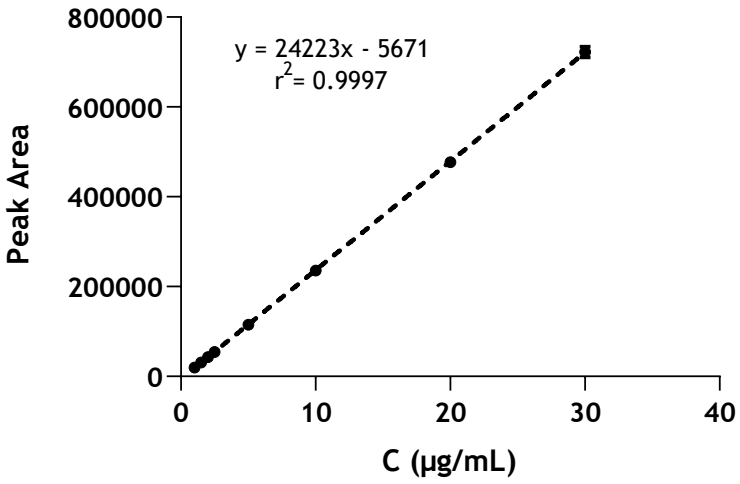


Figure 6 - Line regression graph of niacinamide (n=3)

Table 6 - Linearity results of niacinamide

Slope	24223
y-intercept	-5671
S_a	96.06
S_b	1288
r	1
r^2	0.9997

These results meet the criteria needed for the validation of the calibration curve; hence it illustrates the method was stable over a concentration range of 1 – 30 µg/mL (Figure 6, Table 6).

4.1.6. Limit of quantification and Limit of Detection

LOQ refers to the lowest concentration of an analyte in a sample that can be accurately measured, where the LOD is used to detect the presence or the absence of an analyte in a sample[118]. LOD and LOQ values were calculated based on from the calibration curve parameters, according to the following formulas:

$$LOD = 3.3 \times \frac{\sigma}{a} \quad (7)$$

$$LOQ = 10 \times \frac{\sigma}{a} \quad (8)$$

As σ is the statistics S_b, the standard deviation of y-intercepts of regression lines, and a is the slope of the calibration curve.

The calculated LOD was 0.18 µg/mL and the LOQ was 0.53 µg/mL.

4.1.7. Accuracy and Precision

The accuracy and precision were determined by analyses of samples at three concentration levels (2.00, 10.0, and 30.0 µg/mL) for intra-day variability and at eight concentration levels (1.00, 1.50, 2.00, 2.50, 5.00, 10.0, 20.0, and 30.0 µg/mL) for inter-day variability measurements. The accuracy and precision, represented by the coefficient variation (CV), were expressed by the following equations:

$$Accuracy\ (\%) = \frac{N_C}{Mean\ M_C} \times 100 \quad (9)$$

$$CV\ (\%) = \frac{s}{Mean\ M_C} \times 100 \quad (10)$$

Where N_C is the nominal concentration (µg mL^{-1}), M_C the measured concentration (µg/mL), and s the standard derivation[119]. Intra-day (within-run) values were obtained by replicate analyses (n = 3) followed by interpolation in calibration curves prepared on the same day. Inter-day (between-run) values were also obtained from 3 independent experiments (n = 3).

The intra-day precision was ≤ 2.8% and accuracy ranged between 96.3 and 113% (Table 7). The inter-day precision was ≤ 5.7 carrageenan-polyvinylpyrrolidone % and accuracy ranged between 94.9 and 115% (Table 8). Both intra- and inter-day precision and accuracy found have acceptable values, because precision for each concentration level, represented as CV, did not exceed 15% and the accuracy ranged was between 85 and 115%.

Table 7 - Accuracy and precision for intra-day variability

Intra-day			
Nominal Concentration (µg mL^{-1})	Measured Concentration		
	Mean (µg mL^{-1})	Accuracy (%)	CV (%)
2.00	2.26	113	2.8
10.0	9.63	96.3	0.9
30.0	30.11	101	0.1

Table 8 - Accuracy and precision for inter-day variability

Inter-day			
Nominal Concentration (μg mL^{-1})	Measured Concentration		
	Mean (μg/mL)	Accuracy (%)	CV (%)
1.00	1.15	115	0.7
1.50	1.67	111	0.9
2.00	2.01	101	5.7
2.50	2.44	97.5	5.4
5.00	4.74	94.9	2.5
10.0	9.61	96.1	1.4
20.0	19.42	97.1	1.4
30.0	29.69	98.9	1.8

4.2. Hydrogels

4.2.1. Optimization of carrageenan-based hydrogels

Hydrogels have been used as biomaterials in many different applications, including scaffolds for tissue engineering, wound dressing and carriers for controlled delivery of bioactive molecules[93]. Topical drug delivery systems can be developed in the form of dusting powders, poultices, plasters, lotions, liniments, solutions, emulsions, suspensions, creams, ointments, pastes, and gels, in which hydrogels are included[120]. This study will target the development of a semisolid gel with a smooth jelly-like appearance.

In hydrogel design there is the possibility to use chemical cross-linkers, which usually confer a more stable and stronger hydrogel structure, due to more permanent bonds when compared with physically cross-linked hydrogels. However, physically cross-linked hydrogels tend to be more biocompatible and safer due to the lack of chemical cross-linkers, which have inherent toxicity. Aiming for a biomedical application, pros and cons of each physical and chemical methods must be taken into account, for the best possible outcomes in terms of physicochemical, pharmacokinetic and pharmacodynamic properties[121].

Some cross-linker agents were thought to improve hydrogel properties. One of the classical crosslinking strategies is the use of EDC which is a biocompatible, non-toxic and water-soluble carbodiimide that is an effectively links to amine groups, and it is further stabilized with N-hydroxysuccinimide (NHS). Since the aim was to use carrageenan and this polymer lacks the necessary amino groups for effectively use EDC/NHS as crosslinking strategy, this strategy could not be used[122]. TPP is also a very well-known crosslinking agent among polysaccharide-based hydrogels[123]. TPP a non-toxic polyanion known for its electrostatic crosslinking capacity, resulting in the formation of ionic cross-linked networks[124]. TPP could be an interesting cross-linker to add to PVP, since it could favor the formation of ionic cross-linked networks, which

would be further involved in the carrageenan structure. Hence, addressing the initial statement of avoiding the use of chemical cross-linkers to prevent eventual toxicological concerns, only the blend between carrageenan and synthetic polymers was further explored, taking advantage of the natural and synthetic properties of these polymers.

In the laboratory, κ-CRG hydrogels were already being developed at different % (w/v), from which it was found that hydrogels with a CRG content of 0.90 - 1% (w/v) had a texture and apparent viscosity suitable for a topical gel formulation (Figure S1). It is known that only κ-CRG and ι-CRG evidence gel-forming ability, however, the former forms firmer gels in comparison with the latter[125]. That being said, CRG 1% (w/v) was used for the proceeding formulations.

Synthetic polymers like PVP and PVA have been explored for preparation of biosynthetic formulations in the form of hydrogels[126,127]. PVP is a biodegradable, biocompatible, water-soluble, and a non-toxic polymer. In addition to being a hydrophilic polymer, PVP has good binding properties and it is essentially chemically inert, temperature-resistant and pH-stable[127]. PVA is a neutral, synthetic, water-soluble, hydrogel forming polymer. Because of its mechanical properties and biocompatibility, PVA is extensively utilized in industrial, biomedical and pharmaceutical applications, like drug delivery systems[95].

From Figure 7, it is observable that gel content greatly influences the appearance and viscosity of the hydrogel. Unlike CRG-PVA hydrogel (Figure 7, F1), the one resulting from the mixture of CRG with PVP has a viscosity and texture apparently suitable for application in the form of a topical gel formulation (Figure 7, F2). CRG-PVP (1:1) was chosen as the base matrix for the final optimized hydrogel formulations. This combination allowed the design of a simple, yet effective, platform to deliver niacinamide.

Composition		pH	Observations
F1	CRG 1% - PVA 1% (1:1)	6.5	Very lumpy
F2	CRG 1% - PVP 1% (1:1)	9.1	Good apparent viscosity, smooth

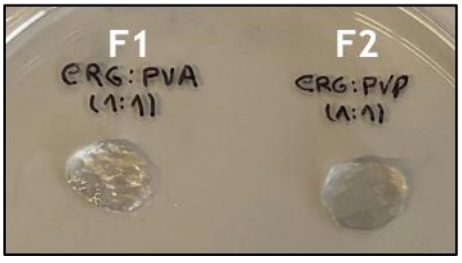


Figure 7 - List and photograph of hybrid hydrogels. F1 (CRG-PVA (1:1)) and F2 (CRG-PVP (1:1)).

One of the most widely implemented approaches to improve drug delivery diffusion and permeation onto the skin is the use of CEs, which ideally act reversibly and temporarily to weaken the barrier resistance of *SC*[128]. Extensive screening and testing have identified different classes of chemicals as CEs, including azone, sulphoxides, pyrrolidones, polyols, alcohols, surfactants, chelating agents, fatty acids, and essential oils[129]. Over the years, natural products have received increasing attention for use as permeation enhancers due to their better safety profile. These products include vegetable oils, which are fixed oils used in cosmetics and medicine, safe to use, and metabolized in the body. They have been found to be effective penetration enhancers due to the presence of fatty acids[130]. In the present study, JO was the vegetable oil selected to act as a permeation enhancer for the final hydrogel formulations.

In the design of the final formulations, different amounts of JO were added (0.5%, 1%, and 5% (w/v)) to the CRG-PVP matrix of the hydrogels. As can be seen from Figure 8, the presence of JO produced hydrogels with an ideal apparent viscosity (Type B and C). In contrast, from Type D hydrogel, it can be noted that a quantity of JO 5% (w/v) is excessive, leading to the saturation of the mixture and the immiscibility of the oil with the two polymers. That said, the latter was not included in the final study.

Composition		pH	Observations
Type A	CRG-PVP (1:1) + NIA 1% (w/w)	8.81	Good apparent viscosity, smooth
Type B	CRG-PVP (1:1) + NIA 1% (w/w) + JO 0.5%	8.99	Ideal apparent viscosity, very smooth
Type C	CRG-PVP (1:1) + NIA 1% (w/w) + JO 1%	8.90	Ideal apparent viscosity, very smooth
Type D	CRG-PVP (1:1) + NIA 1% (w/w) + JO 5%	8.97	JO did not dissolve

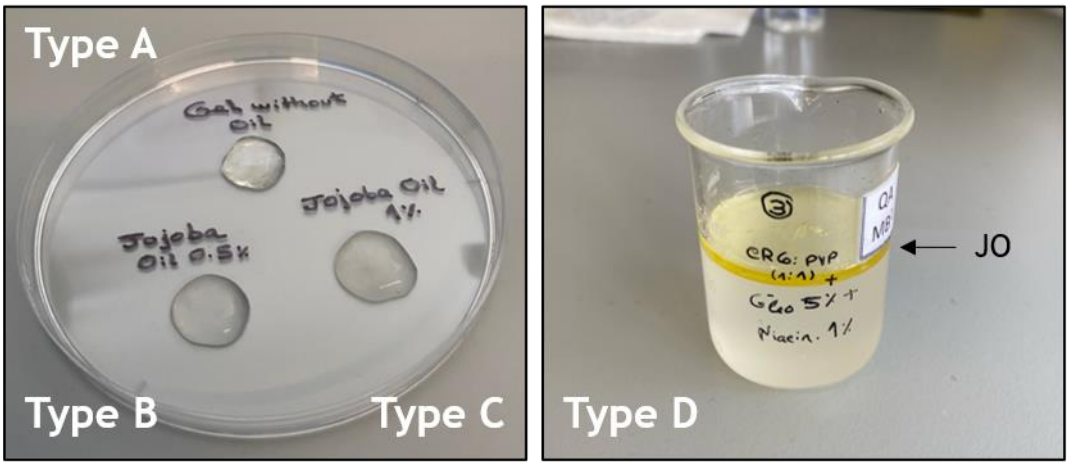


Figure 8 - List and photographs of final hydrogel combinations. Type A (CRG-PVP (1:1) + NIA 1% (w/w)), Type B (CRG-PVP (1:1) + NIA 1% (w/w) + JO 0.5%), Type C (CRG-PVP (1:1) + NIA 1% (w/w) + JO 1%) and Type D (CRG-PVP (1:1) + NIA 1% (w/w) + JO 5%).

The optimized formulated hydrogels that proceeded to the stages of characterization and determination of the permeation profile of niacinamide were Type A, B and C.

4.2.2. Fourier-transform infrared spectroscopy evaluation

To provide evidence on the interaction of the two polymers and incorporation of NIA upon hydrogel production, infrared spectroscopy was performed. The characteristic peaks of the analyzed compounds are detailed in Figure 9, and spectra are given in the range 600-4000 cm^{-1}.

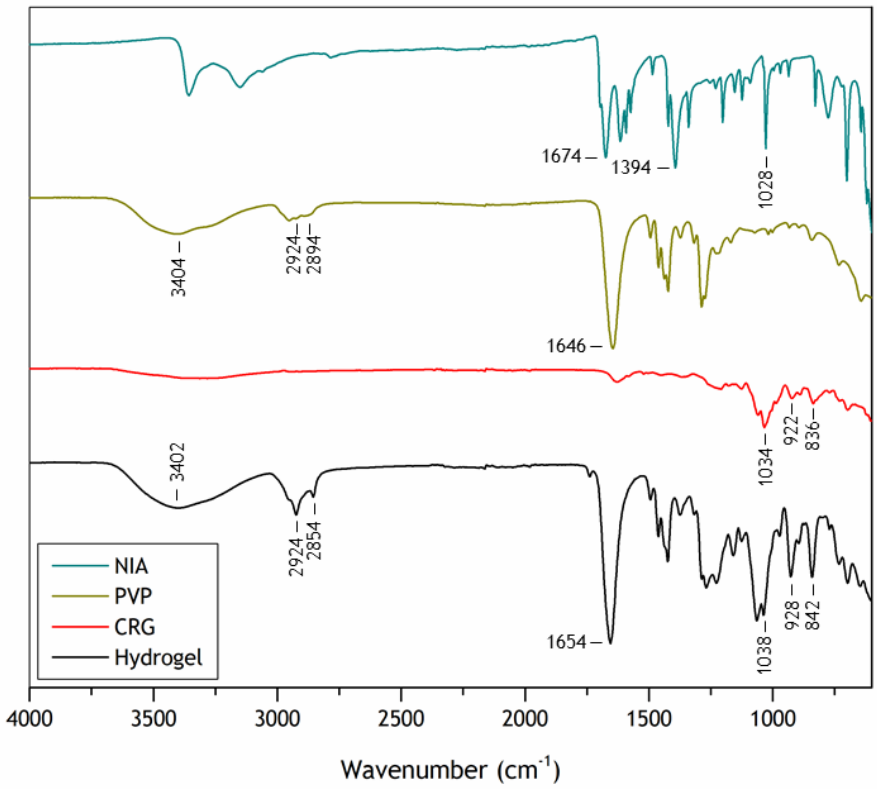


Figure 9 - The FTIR spectra of CRG-PVP NIA-loaded hydrogel (Type A) and all reference compounds.

From the analysis of Figure 9, it is possible to monitor the presence of CRG, PVP, and NIA in the hydrogel matrix. The typical spectrum of CRG with characteristic peaks at 1034, 922, and 836 cm^{-1} (C-O-C stretching, C-O-C of 3,6-anhydrous galactose, and C-H rocking, respectively), can be observed[131]. The characteristic peaks of PVP are present at 3404, 2924, 2894, and 1646 (C-O stretching, asymmetric CH_2 stretching of pyrrole ring, symmetric chain CH_2 stretching, and C=O stretching, respectively)[132]. In the FTIR spectrum of CRG-PVP hydrogel, the bands corresponding to major functional groups belonging to both components can be seen. These

results indicate that synthetic polymer PVP is miscible with the natural polymer CRG. It has been shown that the frequency of C=O stretch is very sensitive to hydrogen bond formation with water molecules[133]. The pyrrolidone rings in PVP contain a proton accepting carbonyl moiety, whereas CRG presents hydroxyl as a hydrogen donor[133]. Therefore, hydrogen bonding interactions may take place between these two chemical moieties in blends of CRG and PVP, as illustrated in Figure 10.

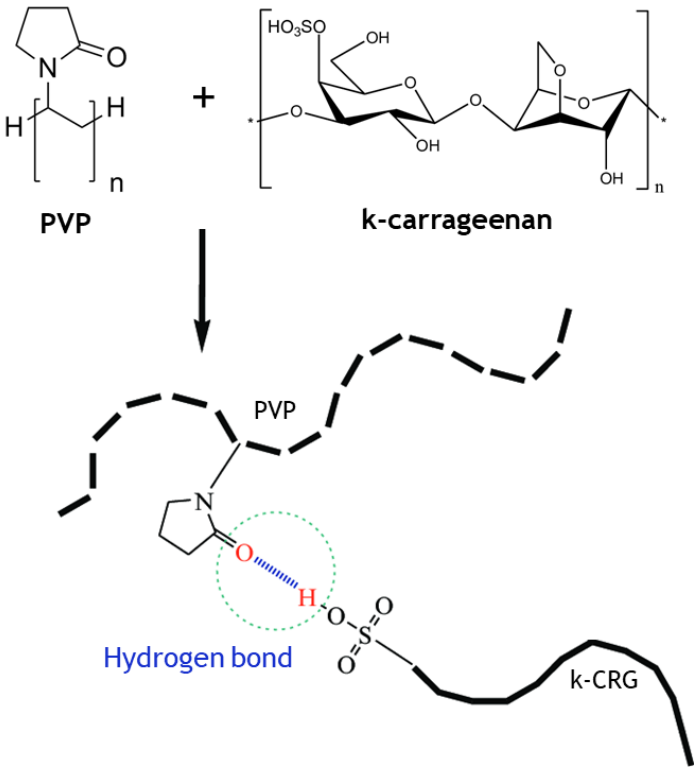


Figure 10 - Schematic representation of hydrogen bonding interactions in the CRG-PVP hydrogel.

As for NIA, the characteristic peaks are evidenced at 3358-3150, 1674, 1394, and 1028 cm^{-1} (asymmetric and symmetric NH2, C=O, C-N, and pyridine stretching, respectively)[134]. The hydrogel is composed of 1% (w/w) of NIA, thus it is important to note that NIA may have to bind in a higher quantity to be quantified by FTIR analysis. However, it may be that the peak at 1038 cm^{-1} in the hydrogel spectrum is representative of the NIA characteristic peak at 1028 cm^{-1}, shifted due to vibrational changes from interactions with the polymers. In addition, the peak at 1654 cm^{-1} in the hydrogel spectrum, may be the result of the peak of NIA at 1674 cm^{-1} masked with the peak of PVP at 1646 cm^{-1}.

To assess the effect of JO in the chemical interactions between CRG, PVP, and NIA in the hydrogel, two hydrogels with different oil percentages, 0.5% and 1% (w/v), were analyzed through FTIR (Figure 11).

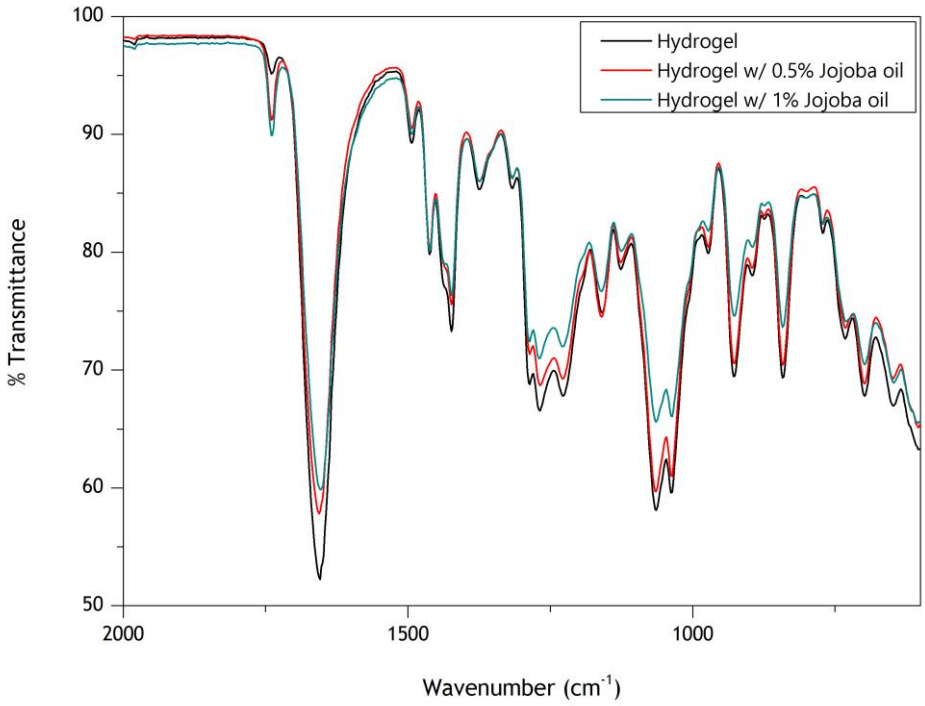


Figure 11 - Evaluation of JO effect on NIA-loaded hydrogel's chemical nature through FTIR.

The coincidence of the FTIR curves in the position of the characteristic frequencies with different JO percentages indicates that the chemical nature of the NIA-loaded hydrogel is kept. Slight changes in the intensity of spectral maxima are observed, which may indicate a change in the quantitative content of the respective functional group in a given frequency. It is known that lower transmittance values at a specific frequency mean increased absorption, due to a higher population of bonds that have vibrational energies corresponding to the incident light[135]. As shown in Figure 11, as the percentage of JO increases, the overall intensity of the characteristic peaks decreases. The FTIR spectra did not show any evidence of interaction between the polymers and the JO.

4.2.3. Morphology evaluation

The morphology assessment of hydrogels was carried out using SEM. From Figure 12, CRG-PVP hydrogel shows a three-dimensional (3D) network structure of porous nature. It appears that the hydrogel presents a robust macrostructure, with rigid walls, observable by the angular fractures resulting from the SEM preparation process. This observation indicates that a proper

combination of CRG and PVP in the hydrogel resulted in the formation of intertwined copolymer hydrogel with a highly linear and aligned network of porous channels. Yacob *et al.*, showed that the mixture of CRG and PVP resulted in the formation of hydrogel with a more regular and porous structure as compared to the structure of the hydrogel of each component alone. Researchers have proven PVP has strengthened the gel and helped in producing a more regular, compact and porous network, as carrageenan alone produced a hydrogel with a non-defined structure[136]. Some artifacts were found on the surface of the hydrogel matrix, with the element in greater quantity being sulfur (S), Figure S2. This may be due to the precipitation of CRG in the form of small crystals during the freeze-drying process.

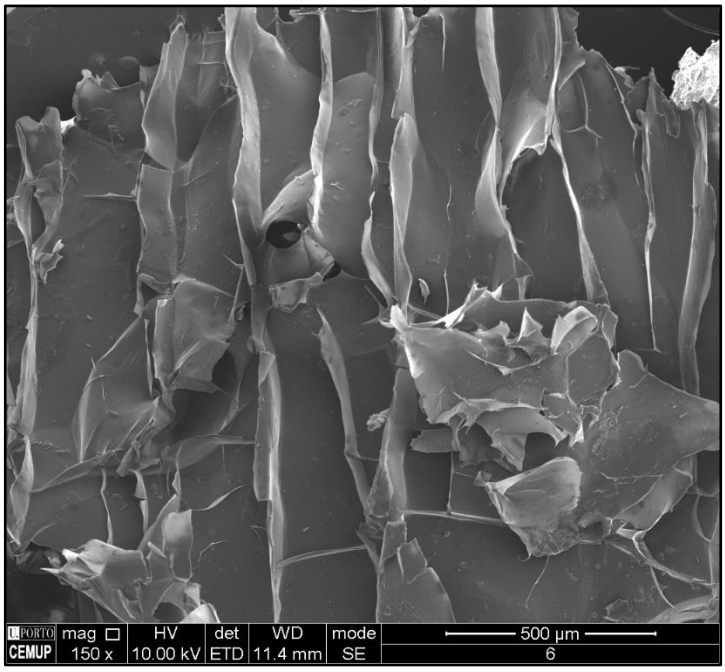


Figure 12 - Morphology of CRG-PVP hydrogel matrix (x150 magnification).

The incorporation of niacinamide in the CRG-PVP hydrogel does not appear to alter the original aligned alveolar macrostructure (Figure 13B). JO does not seem to influence the size and shape of the porous co-polymer hydrogel structure; however, its presence is clear, as it appears to be deposited in the form of a smooth coating, leading to the formation of bubbles on the surface (Figure 13C and Figure S3). As the amount of JO increases in the composition, the oil appears to adopt a patch shape on top of the hydrogel surface. It is noticeable the high affinity that this essential oil has for the polymer matrix, as its accumulation is visible in the area where the alveoli walls merge (Figure 13D).

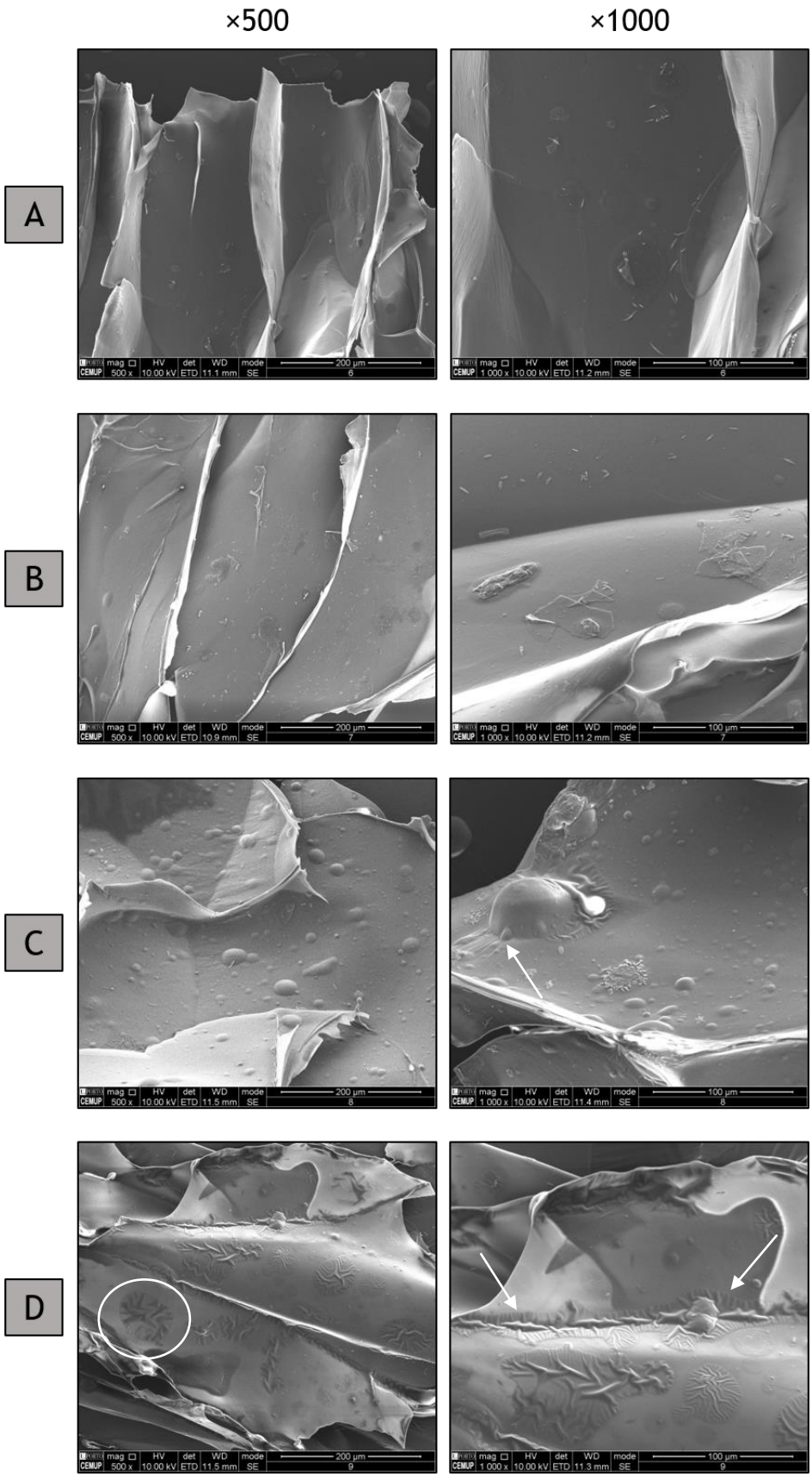


Figure 13 – Influence of JO in hydrogels morphology by SEM. (A) CRG-PVP hydrogel, (B) CRG-PVP NIA-loaded hydrogel, (C) CRG-PVP NIA-loaded hydrogel w/ 0.5% of JO, and (D) CRG-PVP NIA-loaded hydrogel w/ 1% of JO (x500 and x1000 magnification).

4.2.4. Swelling

The evaluation of the swelling profile of hydrogels gives information regarding the bioactive molecule release patterns from these polymeric networks. The rate and degree of swelling are related to crosslinking and mechanical strength of the hydrogels, and depend on the medium (e.g., salts, acids, and bases). Whereas PVP is a not thermo- or pH-sensitive polymer, k-CRG is influenced by the temperature, pH and the presence of cation species, as its degradation occurs through ionic exchanges with surrounding media, reorienting the hydrogel conformation from ordered to disordered[137]. It is known that k-CRG is susceptible to depolymerization in an acidic environment, at pH below 3, as glycosidic linkages are hydrolyzed through acid-catalyzed hydrolysis, leading to partially or complete dissolution of the hydrogel[138]. That being said, the CRG-PVP hydrogels w/ JO were assessed for swelling profile, by measuring the weight of swelled hydrogels at different time points, in sodium chloride solution at neutral pH (7.4 w/ NaCl) and in an aqueous solution at basic pH (9 w/ H_2O) – Figure 14.

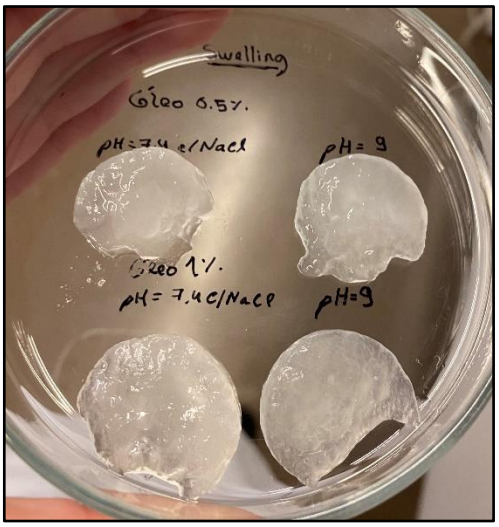


Figure 14 – Photograph of JO hydrogels swelling behavior under neutral salt and basic conditions.

Beforehand, all of the CRG hydrogels from the optimization process were subjected to the swelling assay, from which it was found that hydrogels dissolved partially or totally at an acidic pH, as expected, and showed a more favorable behavior at neutral saline and basic pH conditions. Figure 14 shows that hydrogels contracted and became more compact, instead of presenting a swelling behavior. The fact that the swelling did not occur may be due to the fact that k-CRG gels are more brittle than other types of CRG hydrogels and are more prone to syneresis[139,140]. This process is defined as the spontaneous contraction of a gel without the application of external forces, resulting in the expulsion of a liquid, counteracting the swelling phenomenon. Nonetheless, the mechanism that gives rise to syneresis in gels is still not clear[139].

Regarding the neutral salt condition, the swelling loss can also be emphasized due to a decrease in the osmotic pressure, resulting from the difference in the mobile ion concentration between gel and aqueous phases, and consequently lowering the water diffusion into the hydrogel matrix.

4.2.5. *In vitro* permeation assay

The purpose of the skin permeation studies was to indicate if the active would result in a topical and/or transdermal delivery. The aim of this study was to deliver niacinamide topically using an optimized CRG hydrogel, in order to treat skin conditions such as ageing. Experimental samples included NIA-loaded CRG-PVP hydrogels, two of them containing different percentages of JO, and a control sample was used in all experiments with free NIA dissolved in water at the same amount as in the formulation samples (50 µg of NIA). Skin permeability was evaluated by quantifying the amount of permeated NIA using HPLC analytic method.

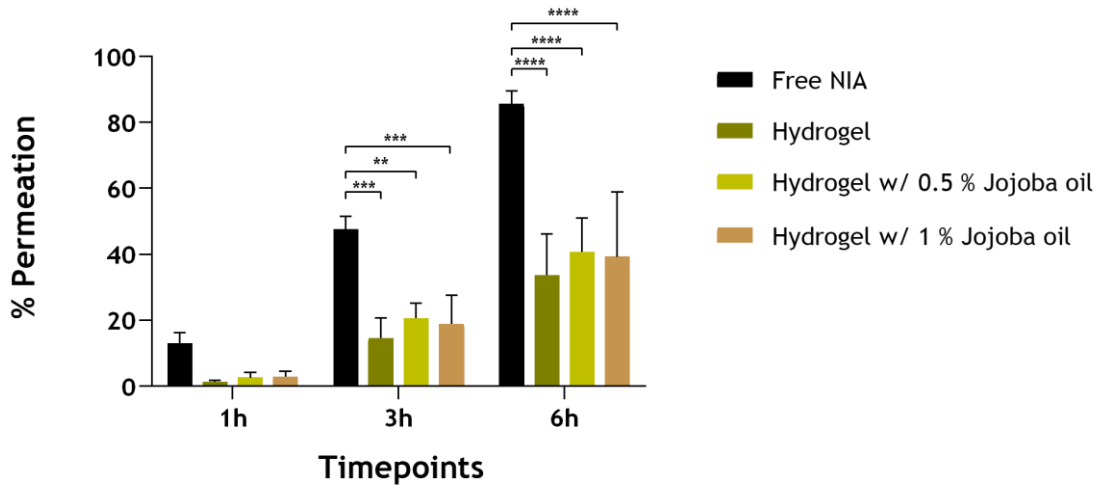


Figure 15 - *In vitro* skin permeation results of free NIA, and NIA-loaded developed hydrogels, from four independent experiments (n=4). Asterisks indicate statistical significance (*, P ≤ 0.05; **, P ≤ 0.01; ***, P ≤ 0.001; ****, P ≤ 0.0001). No asterisks indicate no statistical significance (P > 0.05).

From Figure 15, the first thing that can be seen is the fact that the permeation of NIA is time-dependent in all conditions, as an increase in the rate of skin penetration is detectable over timepoints. Surprisingly, free NIA has a wide permeation capacity, since after 6 h the molecule permeated about 80%. This is not the ideal scenario, as the results demonstrate that NIA alone easily crosses all layers of the skin, reaching blood circulation, and potentially inducing a more systemic effect rather than a controlled topical outcome, as intended. Although NIA is a hydrophilic compound with a log P value of −0.37, the ability of the molecule to penetrate the

skin after topical application has been confirmed by several in vitro studies using human or porcine skin [141-143].

Variability within this type of assay is explained, not only due to the fact that porcine skin is obtained from different healthy animals between independent experiments, but also to long-term storage, the skin lacks viability and enzymatic activity, resulting in variations in the skin permeation[37].

Through the analysis of the results, it appears that there are no significant differences in the permeation capacity of the different formulated hydrogels. Although natural permeation enhancers are known to reduce the lag time of penetrant molecules by reducing the diffusional path length of molecule due to changes in *SC*, JO in these amounts does not appear to alter the ability of NIA to diffuse through the skin[130]. However, they promote a controlled permeation of NIA over time, as after 3 h and 6 h we have a permeation rate of about 20% and 40%, respectively. After 6 h, the permeated NIA concentration varies between 2 - 4 µg / mL, a range of values that does not appear to have biological therapeutic relevance.

4.3. Transethosomes

4.3.1. Formulation and characterization of transethosomes

The present study presents the design, development and characterizing of transethosomes as novel lipid vesicles containing both ethanol and an edge activator or permeation enhancer, which mimic and merge the properties of both ethosomes and transferosomes[102]. Many edge activators have been widely studied in transferosomes composition, including Tween 20, Tween 60, Tween 80, Span 60, Span 65, Span 80, dipotassium glycyrrhizinate, sodium cholate, and sodium deoxycholate, which destabilize the lipid bilayer of liposome systems and increase their flexibility[102]. Oleic acid and jojoba oil have been widely used as permeation enhancers in dermal research to enhance the diffusivity capacity of molecules by disordering the highly packed SC intercellular domain lipids[130,144].

Three different types of transethosomes were prepared by the thin-film hydration method, as previously described. The different compositions differ in the presence of either an edge activator, Tween-80 (Type I formulation), or a permeation enhancer, oleic acid (Type II formulation), and jojoba oil (Type III formulation). While Tween-80 and oleic acid have already been studied in compositions for TEs, jojoba oil is an innovative approach and was selected not only for its composition in fatty acids, known for being good permeation enhancers, but to evaluate its effect on TEs, since its influence was studied in the developed CRG-PVP hydrogels[130]. Non-loaded TEs and formulations containing 30 mg of NIA were physicochemical characterized and the results are summarized in Table 9 and Table 10, respectively.

From Table 9, the DLS measurements show that the unloaded formulations presented an average size of 133 ± 1, 320 ± 27, and 249 ± 4 nm, regarding Type I, II, and III respectively, which is within the adequate size range for topical delivery[145]. The polydispersity index for the prepared nanoparticles was below 0.3 for Type I and Type III, and close to 0.3 for Type II. Danaei *et al*. stated that a population of phospholipid vesicles is homogeneous and monodispersed if the PDI value is lower than 0.3, thus, these results represent adequate values of formulations with a narrow range of particle size[146]. Table 9 data evidenced zeta potential values of -15 ± 3, -31 ± 1, and -19 ± 1 mV for Type I, Type II, and Type III TEs, respectively, indicating the need to verify stability during storage, especially for Type I and III. It is well established that when surface values are equal to or higher than |30| mV, the nanoparticles have electrostatic stabilization and a low tendency to aggregate[147]. These results are expected since Tween-80 (Type I) is a non-ionic surfactant, does not carry a net charge, resulting in lower ZP magnitude values[148,149]. Moreover, the high zeta potential value of Type II TEs may be explained by the fact that oleic acid is negatively charged in a water environment with a neutral pH[150].

Table 9 - Characterization of non-loaded TEs Type I, II, and III.

	PS (nm)	PDI	ZP (mV)
Type I	132 ± 1	0.290 ± 0.002	-15 ± 3
Type II	320 ± 27	0.316 ± 0.011	-31 ± 1
Type III	249 ± 4	0.250 ± 0.011	-19 ± 1

Each value represents the mean ± SD of 2 independent measurements (n=2). PS – particular size; PDI – polydispersity index; ZP – zeta potential; EE – encapsulation efficiency; LC – loading capacity.

Table 10 shows that incorporation of NIA did not affect PS values, as all formulations present an ideal hydrodynamic size range. Nonetheless, upon loading with NIA, a reduction of TE Type II size and ZP is noticeable. This may be due to the fact that NIA, in the presence of oleic acid, leads to a rearrangement of phospholipids of this liposomal-type system and, thus, to a reduction of the size of the vesicle. All loaded-TEs show a fairly narrow size distribution and good dispersion (PDI value ≤ 0.3). Table 10 data evidenced zeta potential values of -17 ± 4, -40 ± 2, and -21 ± 6 for Type I, Type II, and Type III TEs, similar to the non-loaded TEs. Transethosomes showed encapsulation efficiency and loading capacity values ranging from 3.9 – 5.6 %, and 5.3 – 7.6 %, respectively, Type III being the most favorable formulation on both parameters.

Tazina *et al*. stated that depending on the hydration conditions and the drug properties, encapsulation efficiency varies from 5 to 20%, using the thin film hydration method to prepare

liposomes, as its efficiency is dependent on liposome internal volume and lipid concentration. The incorporation of a water-soluble molecule into a liposome system can be improved by a dehydration-rehydration process, to improve the loading[151]. In the present study, since transethosomes are liposome-like vesicular systems, the TE composition allied to the possible low efficient method may be causing the low EE% values.

Moreover, Colletier *et al.* showed that using the thin film hydration method, the encapsulation efficiency of a protein was dependent on the interaction between the molecule and the lipid bilayer. The best way to increase EE was by manipulation of liposomal lipid composition and by increasing lipid concentration, in order to favor electrostatic interactions, hence the highlighted importance given to the ionic strength of the enzyme solution[152]. In the present study, NIA could be hindering electrostatic interactions due to partial charges, preventing a higher encapsulation efficiency.

Table 10 - Characterization of loaded-TEs Type I, II, and III.

	PS (nm)	PDI	ZP (mV)	EE (%)	LC (%)
Type I	132 ± 9	0.295 ± 0.006	-17 ± 4	3.9 ± 0.9	5.3 ± 1.2
Type II	171 ± 18	0.296 ± 0.020	-40 ± 2	4.9 ± 1.6	6.7 ± 2.2
Type III	215 ± 6	0.232 ± 0.010	-21 ± 6	5.6 ± 1.8	7.6 ± 2.5

Each value represents the mean ± SD of 3 independent measurements (n=3). PS – particular size; PDI – polydispersity index; ZP – zeta potential; EE – encapsulation efficiency; LC – loading capacity.

4.3.2. Fourier-transform infrared spectroscopy evaluation

The FTIR analysis was performed after freeze-drying nanoparticles to validate the NIA incorporation into the lipid nanoparticles, and the characteristic peaks of the analyzed compounds are detailed in Figure 16. As represented in the spectra of NIA, the characteristic peaks are evidenced at 3356-3148, 1674, and 1394 cm^{-1} (asymmetric and symmetric NH2, C=O, and C-N stretching, respectively)[134]. As expected, the spectrum of non-loaded TEs is very similar to the spectrum of EPC, which is mainly characterized by peaks at 1092 cm^{-1} (P=O stretching); 1733 cm^{-1} (C=O stretching); and 2922 and 2822 cm^{-1} (CH2, CH3 stretching in the fatty acid part of the EPC structure)[112]. The combination of characteristic peaks of EPC and free NIA appears in the spectrum of NIA-loaded transethosomes, and no new bonds appear, indicating that niacinamide was successfully incorporated without altering its chemical structure or the structure of the nanoparticles. This was also verified in Type II and Type III formulations (Figure S4 and Figure S5).

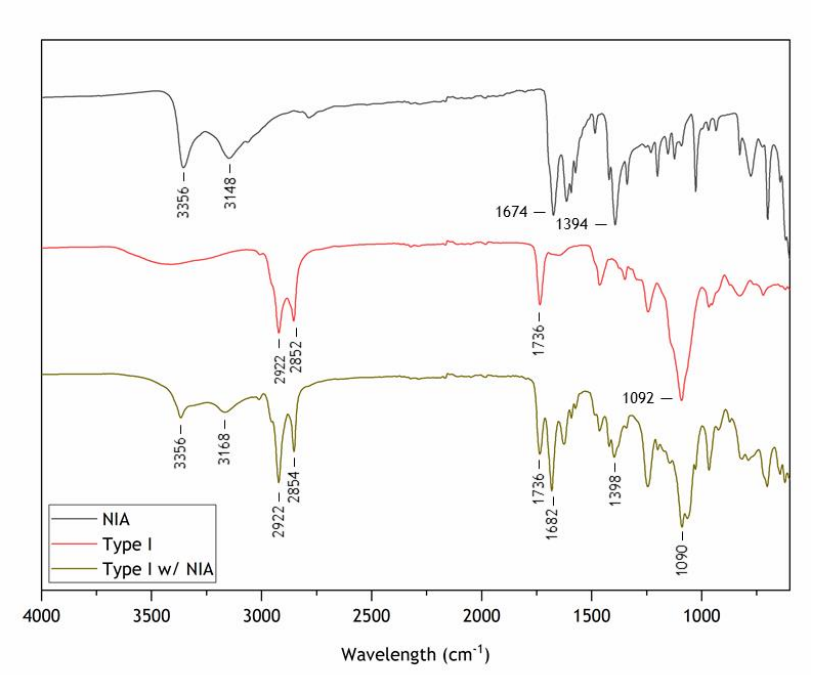


Figure 16 - The FTIR spectra of reference compound (NIA) and nanoformulations (Type I and Type I w/ NIA).

Figure 17 shows that the main characteristic molecular vibrations of the EPC transethosomes are kept, regardless of the presence of an edge activator, Tween-80, or a permeation enhancer, like oleic acid and jojoba oil on Type I, II, and III, respectively.

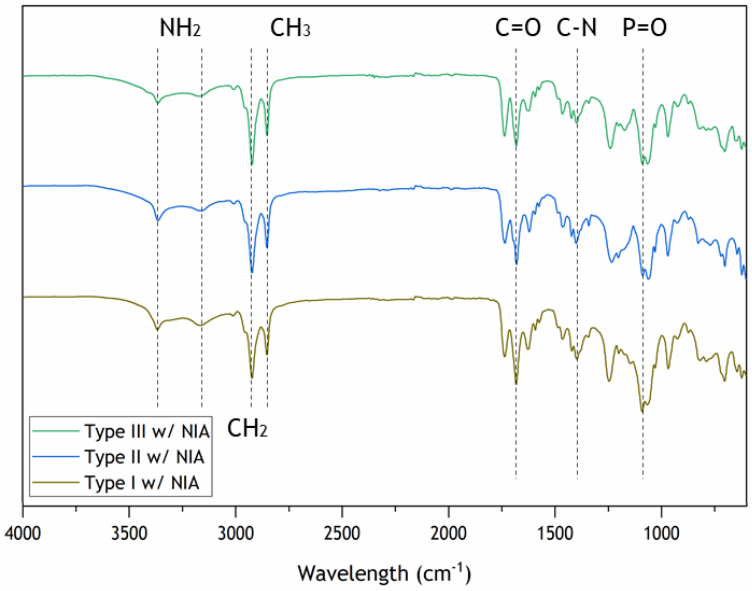


Figure 17 - FTIR spectra of Type I, II, and III formulations, containing NIA.

4.3.3. Morphology evaluation

The morphology of the nanoparticles was assessed by using TEM and the results are displayed in Figure 18. Overall, all formulations have nanoparticles with an almost spherical shape, the typical liposome structure[153]. As expected, since NIA is a small bioactive compound, its incorporation did not affect the shape nor the size of the nanoparticle. Moreover, in Type II, oleic acid may be the compound forming the wire-like structures that can be observed in the lipid bilayer zone. When aggregations are visible, the spherical shape becomes more irregular, which emphasizes the high deformability of TEs membrane that enables them to adapt its form to the surrounding space (Type I w/ NIA and Type III)[154]. However, it is possible to observe from the images that TEs Type III are more predisposed to the formation of aggregates, in comparison with the other types.

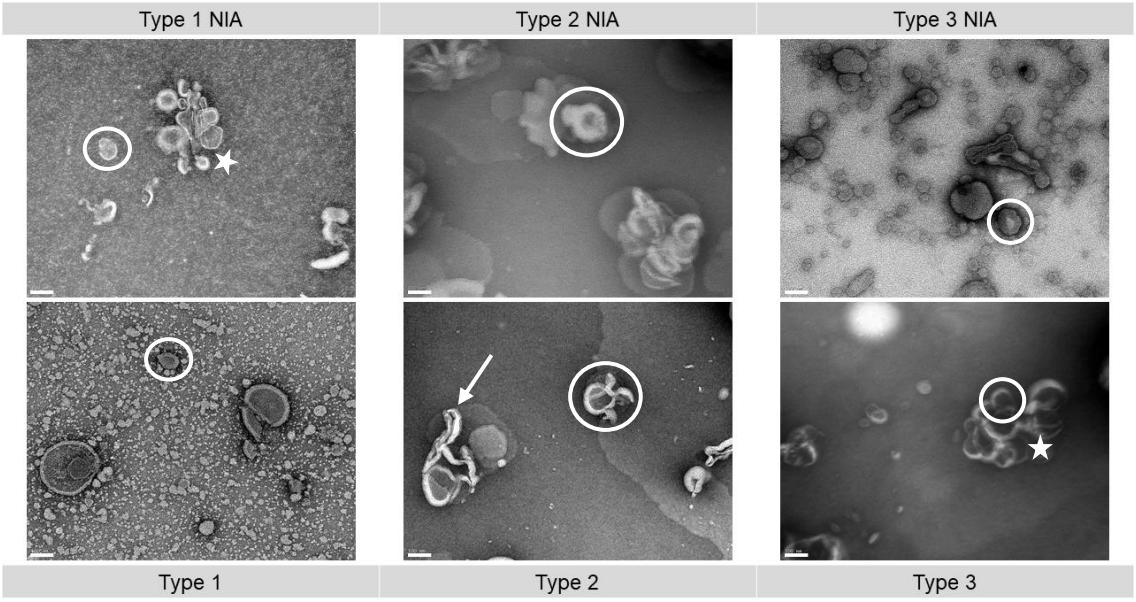


Figure 18 - Non-loaded and NIA-loaded TEs morphology. Transmission electron microscopy images obtained for Type I, Type II, and Type III TEs (×100000 magnification). (Circle: size and shape; Arrow: wire-like structure; Star: aggregate). Scale bar: 100 nm.

4.3.4. Stability assessment

Formulations were kept at 4ºC and storage stability was evaluated in terms of particle size, PDI and zeta potential over 2 weeks. Figure 19 shows that PS and ZP of loaded TEs remain practically constant during the period of study at 4ºC temperature. Regarding the polydispersity index, in all NIA-loaded formulations it is possible to find the same trend towards lower values, below 0.3, suggesting low tendency for aggregation. Stability does not seem to be affected when considering data from size, PDI and ZP, in non-loaded TEs (Figure S6).

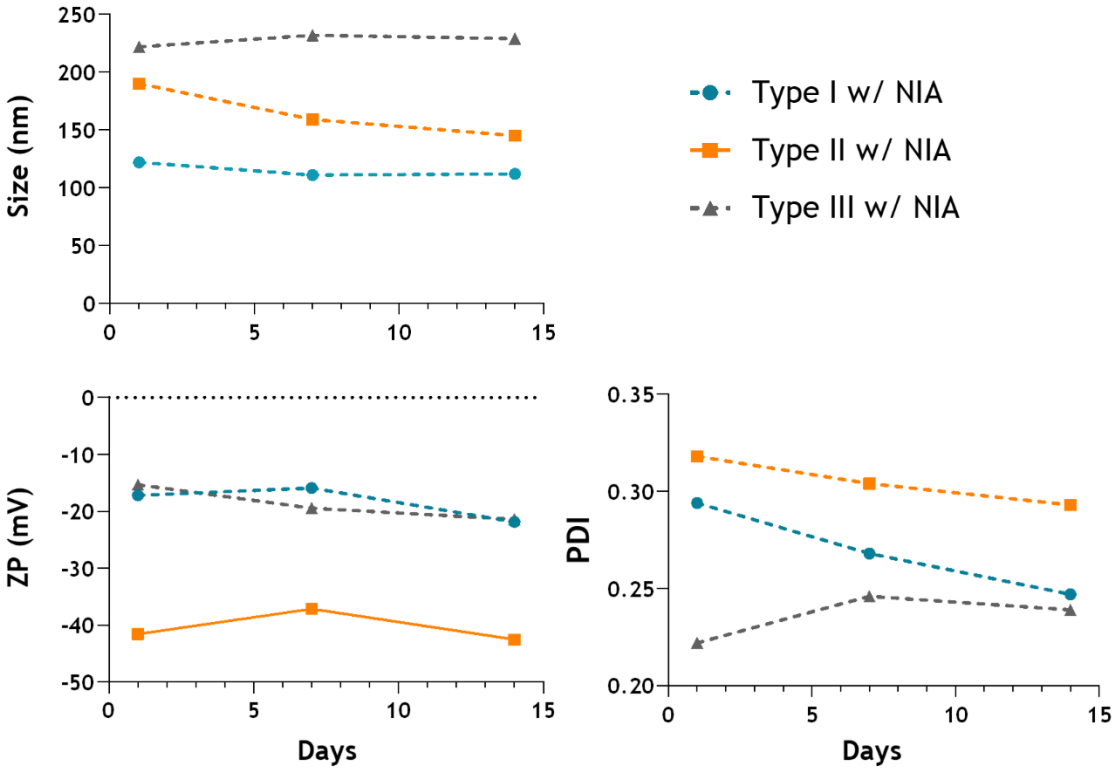


Figure 19 - Storage stability of NIA-loaded formulations at 4°C over 2 weeks. Size, zeta potential and polydispersity index values displayed (Size: SD<2%; ZP: SD<5%; PDI: SD<3%).

The stability of the formulations was also assessed by performing measurements of EE% and LC% values after 2 weeks – Figure 20. It can be seen that Type II TEs showed a reduction of these values by half. That said, it appears that formulations composed of oleic acid are less stable, compared to the other two types.

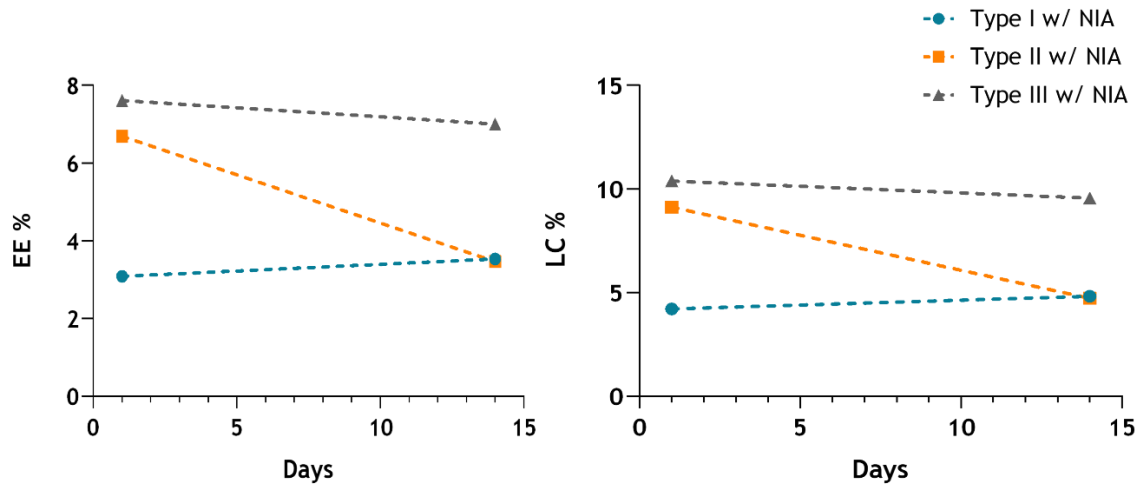


Figure 20 - Storage stability of NIA-loaded formulations at 4°C over 8 weeks. EE% and LC% values displayed.

4.3.5. *In vitro* permeation assay

Transethosomes loaded with NIA were developed as a second delivery system, besides hydrogels, to enhance the permeation capacity of NIA. To determine the skin permeability of NIA-loaded TEs, a control sample was prepared using Milli-Q water (pH 7.4) as a solvent for NIA, whereas experimental samples were transethosomes (Type I, II, and III). Skin permeability was evaluated by quantifying the amount of NIA that had penetrated the skin using a Franz diffusion cell and HPLC analysis. Results are shown in Figure 21.

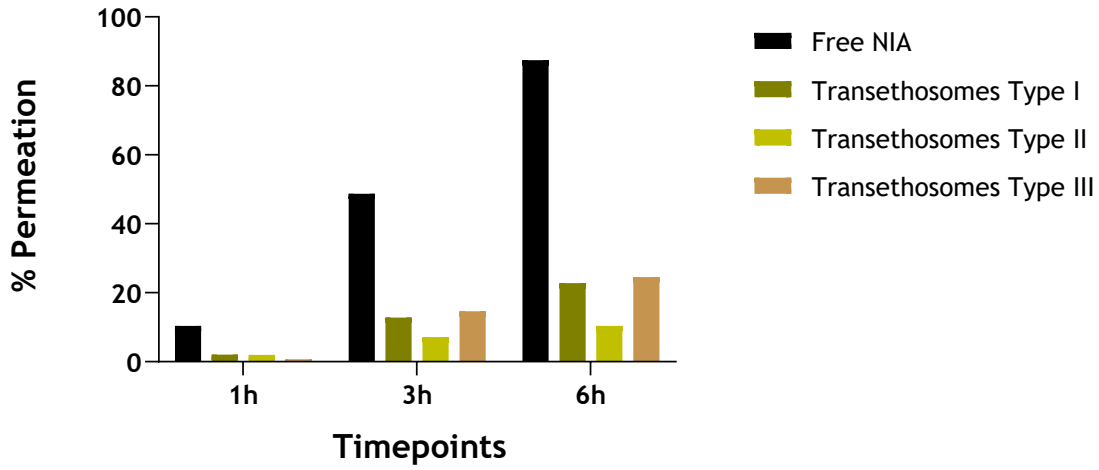


Figure 21 - *In vitro* skin permeation results of free NIA, and NIA-loaded TEs (Type I, II, and III), from one experiment (n=1).

Two independent experiments were carried out (n = 2), however, given the variability observed for one formulation, one assay is presented to evident the performance of the NIA-loaded TEs. From Figure 21, it can be seen that transethosomes follow the same tendency as hydrogels (Figure 15), pendent experiments will have to be carried out in the future to obtain a statistically valid pattern.

As previously seen in the permeation assays with CRG-PVP hydrogels, free NIA has a cumulative permeation rate that reaches about 80% after 6 h, which is not suitable for the intended topical effect, as it indicates that the compound alone penetrates and permeates through the skin layers in an uncontrolled way, in a considerable speed. In contrast, TEs have a more controlled permeation rate of NIA, about four times lower, compared to free NIA. After 1 h, it is still not possible to observe significant differences concerning the various types of TEs developed, however, after 3 h and 6 h, it is observed the effect that Tween-80 (Type I) and jojoba oil (Type III) have in the ability of these NPs to permeate.

It should be noted that TEs are more effective at retaining NIA in the skin layers, since hydrogels seem to penetrate and permeate the skin more easily.

4.4. Transethosomes-loaded hydrogels

The innovative combination of these two drug delivery systems was thought to evaluate possible permeability enhancements from the hydrogel and/or transethosome. To determine the skin permeability of TEs-loaded hydrogels, CRG-PVP hydrogel w/0.5% JO was selected to incorporate the NIA-loaded TEs (Type I, II, and III). The choice of the hydrogel was based not only on the respective *in vitro* permeation assays, but also on the amount of JO (0.5%), since the transethosomes are also composed of an edge activator or permeation enhancer. Results are shown in Figure 22.

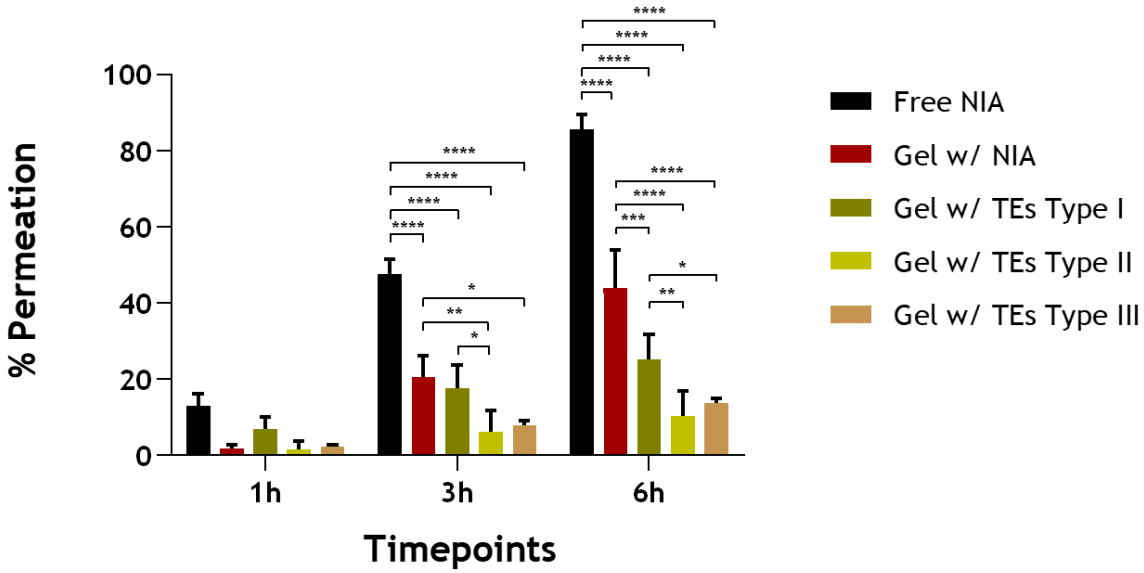


Figure 22 - *In vitro* skin permeation results of free NIA, NIA-loaded hydrogel, and TEs-loaded hydrogels (Type I, II, and III), from three independent experiments (n=3). Asterisks indicate statistical significance (*, P ≤ 0.05; **, P ≤ 0.01; ***, P ≤ 0.001; ****, P ≤ 0.0001). No asterisks indicate no statistical significance (P > 0.05).

From Figure 22, it can be seen that NIA-loaded hydrogels lead to higher drug permeation comparing to NIA-loaded TEs incorporated within hydrogels. After 1 h, although the differences are not significant, there is a certain prominence of the hydrogel containing TEs Type I, whose permeation rate slowly increases over time, being surpassed by the permeation capacity of the hydrogel alone. Nevertheless, NIA-loaded TEs Type I hydrogel capacity to permeate NIA is always superior to the other two types of TEs incorporated within hydrogel. Comparing these results to those of the permeation assay with TEs only, the values are similar, except when using Type III TEs. The combination of hydrogel with TE Type III appears to hamper the ability to permeate NIA, which may be due to the fact that both delivery systems have a certain amount of JO, resulting in a saturation limit of the combined system.

It is important to point out that hydrogels alone have a superior permeation, comparing not only to the transethosomes alone, but also to the combination of the two delivery systems together.

4.5. Apparent Permeability Comparison

Table 11 summarizes the apparent permeability coefficients of Free NIA and all NIA-loaded formulations developed in this study, to analyze the appearance rate of the compound in the receiver compartment, at time point 3 h. As expected, these results are in accordance with the values obtained from the permeation assays performed. Comparing to the control (Free NIA), it is clear that all formulations have a more controlled permeation capacity, as the appearance rate of NIA is less than half in all cases. From Table 11, among all the formulations it is clear that TEs are more effective at retaining NIA in the skin layers, for the intended topical effect. However, due to their viscosity, they cannot be applied alone. Given the consistency and storage stability of the TEs incorporated within CRG-PVP hydrogels, the NIA permeated and the P_{app} values, the combination of the hydrogel with TEs Type III is the best option for the topical anti-ageing effect intended.

Table 11 - Apparent permeability coefficient of Free NIA and NIA-loaded formulations across the *in vitro* skin barrier

Composition	P_{app} ($\times 10^{-5}$ cm/s)
Free NIA	6.49 ± 0.99
Hydrogel	2.13 ± 0.90
Hydrogel w/0.5%JO	3.01 ± 0.66
Hydrogel w/ 1% JO	2.77 ± 1.25
Type I TEs	1.87
Type II TEs	1.04
Type III TEs	2.13
Hydrogel (0.5% JO) w/ Type I TEs	2.58 ± 0.87
Hydrogel (0.5% JO) w/ Type II TEs	0.90 ± 0.81
Hydrogel (0.5% JO) w/ Type III TEs	1.17 ± 0.17

Each value represents the mean ± SD of 4 independent measurements for hydrogels (n=4), 1 measurement for transethosomes (n=1), and 3 independent measurements for combination of both (n=3).

5. Concluding remarks

Drug delivery via the skin is becoming progressively popular and has now established a place in the pharmaceutical and cosmetic industry. The skin acts as an ideal site to deliver the drug both locally and systemically, to achieve controlled and prolonged drug delivery[32]. Topical and transdermal drug delivery systems have shown significant advantages in clinical practice due to their convenience, affordability, and most importantly, targeting the drug to the intended action site in the body[14].

Considering niacinamide for topical application, the physicochemical characteristics of the bioactive compound, as well as the physicochemical properties of the skin must be taken into consideration. The skin provides an effective physical barrier between external stressors and the inner system, and its barrier function mainly resides in the *stratum corneum*, which represents a major challenge in the cutaneous administration of drugs, in clinical practice[15].

Drug's bioavailability and biodistribution across the skin layers are mainly dependent on molecular size, solubility, ionisation, and the partition coefficient of the molecule[57]. The ideal molecular weight for a molecule penetrating intact *SC* should be less than 500-600 Da and the action itself should present a biphasic solubility[59,60]. When considering the ionisation of the active, the ionized form of the molecule is less likely to penetrate in comparison with the non-ionized[62]. The partition coefficient of bioactive compounds with values below 1 are too hydrophilic and have difficulties diffusing through the *SC*[64]. Although NIA is a small molecule with a size of 122.1 Da, it is extremely soluble in water (212.95 mg/mL), completely ionized in physiological conditions (pKa 3.35), and has a log P value of – 0.37, which indicates that this active alone may not be ideal for topical delivery[72].

For these reasons, the major goal of this thesis was to explore the topical skin delivery of NIA by formulating, optimizing, and characterizing two drug delivery systems to mask niacinamide's physicochemical properties. Herein, we aimed at further exploring this by **i) validating and implementing a quantification method for niacinamide**; **ii) design, optimization, and characterization of carrageenan-based hydrogels; iii) formulation and characterization of transethosomes**; **iv) formulation of the optimized carrageenan-based hydrogel containing the transethosomes**; v) **determination of the skin permeation profile of the developed delivery systems**, to quantify the amount of permeated NIA.

Optimization of CRG-hydrogel composition led to the design of three formulations with a CRG-PVP matrix, differing only in the amount of JO present. It was noticeable that there was a limit of saturation for the amount of JO used, with 5% w/v being excessive and causing the enhancer to be immiscible with the polymers. The physicochemical characterization of the optimized hydrogels was made through FTIR, morphology, and swelling assessment. In the analysis of the

chemical interactions established in the hydrogel, it was possible to conclude not only the miscibility of the natural polymer CRG and the synthetic polymer PVP, which established hydrogen bonding interactions when forming the matrix, but also, the incorporation of NIA and the fact that JO did not affect the hydrogel's chemical nature. The morphology assessment made clear the formation of a robust macrostructure with a highly linear and aligned network of porous channels, based on the CRG-PVP matrix, which was not affected by the incorporation of NIA. Moreover, the presence and the high affinity of JO to the polymer matrix were verified. The swelling assay showed that a syneresis phenomenon had occurred, which counteracted the swelling behavior, resulting in a contraction of the matrix and not in its expansion.

In vitro skin permeation assays with hydrogels allowed us to conclude that the developed formulations are an effective delivery system, as they promote a controlled permeation of niacinamide over time. Although there are no significant differences in the permeation capacity between the different hydrogels used, and therefore, the non-influence of JO, after 6 h, it is possible to observe a permeation rate of about 40%. From which it can be concluded that hydrogels enhance NIA's penetration and permeation in a controlled manner, but still allow the retention of an adequate amount of NIA in the layers of the skin. Surprisingly, the control sample (NIA dissolved in water) showed an exacerbated permeation rate, contradicting the fact that some physicochemical characteristics of NIA hinder its topical administration.

Transethosomes development led to the design of three different formulations, using distinct surface-active agents: a non-ionic surfactant, Tween-80, for Type I formulation; a well-known permeation enhancer, oleic acid, for Type II formulations; and a natural enhancer with a vegetable origin, jojoba oil, for Type III formulations. Loaded-transethosomes were formulated to contain 30 mg of niacinamide and physically characterized by performing measurements of PS, PDI, ZP, EE%, and LC%. The size of the three types of TEs ranged from 133- 215 nm, an ideal hydrodynamic size range for topical application, and the PDI values were ≤ 0.3. The TEs had ZP values of -17, -40, and -21 mV for Type I, Type II, and Type III TEs, respectively. It can be concluded that whilst oleic acid confers the lowest and most stable value of ZP, due to its negatively charged ionized form in a neutral aqueous environment, Tween-80, as a non-ionic surfactant with uncharged hydrophilic group, prompts the charge at the interface between the TE external surface and the aqueous medium to neutral values[148-150]. As expected, these values did not differ significantly from the non-loaded TEs measurements, taking into account that NIA is a small molecule with a hydrophilic nature that lodges in the inner space of the nanoparticle. TEs EE% and LC% values ranged from 3.9 – 5.6%, and 5.3 – 7-6%, respectively, type 3 being the most favorable formulation on both parameters.

Stability assessment allowed the conclusion that formulations had no tendency to aggregate, as the PDI values decreased over the study period, and the values related to size and ZP did not undergo significant changes. However, Type II TEs proved to be the least stable

formulation, as the EE% and LC% values decreased to half in two weeks. FTIR analysis validated the successful incorporation of NIA into the lipid NPs, without altering its chemical structure or the structure of the TEs. Beyond this, FTIR characterization allowed the conclusion that regardless of the presence in the composition of an edge activator or a permeation enhancer, TEs' chemical nature was kept.

In vitro permeation assays with transethosomes allowed us to conclude that they are more effective at retaining NIA in the skin, comparing to NIA-loaded hydrogels, which penetrate and permeate more easily. After 6 h, TEs showed a cumulative permeation rate of about 20% for Type I and Type III, and 10% for Type II, practically half of the results obtained with hydrogels.

Overall, it may be said that these nanoparticles are more effective at retaining NIA in the skin layers, comparing to the optimized CRG-hydrogels, for the topical anti-ageing effect intended. However, further tests have to be carried out to establish a statistically valid pattern for TEs permeability capacity.

Skin permeation studies with TEs-loaded hydrogels showed that the combination of the two drug delivery systems resulted in an adequate controlled permeation of NIA. It allowed us to conclude that NIA-loaded hydrogels not only lead to higher drug permeation values comparing to TEs alone, but also to the combination of both delivery systems together. After 6 h, TEs-loaded hydrogels showed a cumulative permeation ranging from 10 – 30 %.

Given the consistency and storage stability of the TEs incorporated within CRG-PVP hydrogels, the NIA permeated and the P_{app} values, the combination of the hydrogel with TEs Type III is the best option, for the topical anti-ageing effect intended.

Collectively, all the main aims of the thesis were tackled. Although some results did not meet our expectations, important steps were taken to show how versatile drug delivery systems can be, and how important is their use for topical applications in a controlled manner. Further studies must be conducted in the optimization involving transethosomes, to unlock their full potential as a tool for cosmetic applications; in the quantification of mass, to determine the exact amount of NIA retained in the skin, and therefore, have a more complete and precise entail; in the determination of free radical scavenging capacity of NIA; and in the determination of drug release profiles.

6. References

1. Lai-Cheong, J. E. & McGrath, J. A. Structure and function of skin, hair and nails. *Med. (United Kingdom)* **45**, 347–351 (2017).
2. Lee, S. H., Jeong, S. K. & Ahn, S. K. An update of the defensive barrier function of skin. *Yonsei Med. J.* **47**, 293–306 (2006).
3. Byrd, A. L., Belkaid, Y. & Segre, J. A. The human skin microbiome. *Nat. Rev. Microbiol.* **16**, 143–155 (2018).
4. Quaresma, J. A. S. Organization of the skin immune system and compartmentalized immune responses in infectious diseases. *Clin. Microbiol. Rev.* **32**, 1–35 (2019).
5. Belkaid, Y. & Segre, J. A. Dialogue between skin microbiota and immunity. *Science.* **346**, 954–959 (2014).
6. Kabashima, K., Honda, T., Ginhoux, F. & Egawa, G. The immunological anatomy of the skin. *Nat. Rev. Immunol.* **19**, 19–30 (2019).
7. Grice, E. A. & Segre, J. A. The skin microbiome. *Nat. Rev. Microbiol.* **9**, 244–253 (2011).
8. Ross, A. A., Rodrigues Hoffmann, A. & Neufeld, J. D. The skin microbiome of vertebrates. *Microbiome J.* **7**, 1–14 (2019).
9. Owens, D. M. & Lumpkin, E. A. Diversification and specialization of touch receptors in skin. *Cold Spring Harb. Perspect. Med.* **4**, 1–12 (2014).
10. Newman, T. Skin: How it works. Retrieved January 22, 2021, from https://www.medicalnewstoday.com/articles/320435#functions (2018).
11. Arens, E. A. & Zhang, H. The skin's role in human thermoregulation and comfort. in *Thermal and Moisture Transport in Fibrous Materials* 560–602 (2006).
12. Wickett, R. R. & Visscher, M. O. Structure and function of the epidermal barrier. *Am. J. Infect. Control* **34**, 98–110 (2006).
13. Fenner, J. & Clark, R. A. F. Anatomy, Physiology, Histology, and Immunohistochemistry of Human Skin. in *Skin Tissue Engineering and Regenerative Medicine* 1–17 (2016).
14. Mishra, D. K., Pandey, V., Maheshwari, R., Ghode, P. & Tekade, R. K. *Cutaneous and transdermal drug delivery: Techniques and delivery systems. Basic Fundamentals of Drug Delivery* (2019).
15. Menon, G. K., Cleary, G. W. & Lane, M. E. The structure and function of the stratum corneum. *Int. J. Pharm.*, vol. 435 3–9 (2012).
16. Andrews, S. N., Jeong, E. & Prausnitz, M. R. Transdermal Delivery of Molecules is Limited by Full Epidermis, Not Just Stratum Corneum. *Pharm. Res.* **30**, 1099–1109 (2013).
17. Thong, H. Y., Zhai, H. & Maibach, H. I. Percutaneous penetration enhancers: An overview. *Skin Pharmacology and Physiology* vol. 20 272–282 (2007).
18. Saifee, M., Rajendra, V. & Dehghan, M. H. G. Physical Approaches to Penetration Enhancement. *Int. J. Heal. Res.* **3**, (2011).
19. Haque, T. & Talukder, M. M. U. Chemical enhancer: A simplistic way to modulate barrier function of the stratum corneum. *Adv. Pharm. Bull.* vol. 8 169–179 (2018).
20. Dragicevic, N., Atkinson, J. P. & Maibach, H. I. Chemical Penetration Enhancers: Classification and Mode of Action. in *Percutaneous Penetration Enhancers Chemical Methods in Penetration Enhancement* 11–27 (2015).
21. Williams, A. C. & Barry, B. W. Penetration enhancers. *Adv. Drug Deliv. Rev.* vol. 64 128–

137 (2012).

22. Chen, J. *et al*. Potential of Essential Oils as Penetration Enhancers for Transdermal Administration of Ibuprofen to Treat Dysmenorrhoea. *Molecules J.* **20**, 18219–18236 (2015).

23. Abdo, J. M., Sopko, N. A. & Milner, S. M. The applied anatomy of human skin: A model for regeneration. *Wound Med.* **28**, (2020).

24. Nafisi, S. & Maibach, H. I. *Skin penetration of nanoparticles*. *Emerging Nanotechnologies in Immunology: The Design, Applications and Toxicology of Nanopharmaceuticals and Nanovaccines* (Elsevier Inc., 2018).

25. Brown, T. M. & Krishnamurthy, K. Histology, Dermis. *StatPearls [Internet]* (2018).

26. Smith, M. M. & Melrose, J. Proteoglycans in Normal and Healing Skin. *Adv. Wound Care* **4**, 152–173 (2015).

27. Debelle, L. & Tamburro, A. M. Elastin: Molecular description and function. *Int. J. Biochem. Cell Biol.* **31**, 261–272 (1999).

28. Junctions, M., Tissue, S., Appendages, S. & Skin, H. O. F. Subcutaneous Tissue. 9–11 (2002).

29. Vitorino, C. S. P. Lipid Nanoparticles and Permeation Enhancement for Transdermal Drug Delivery. (University of Coimbra, 2013).

30. Montoto, S. S. & Ruiz, M. E. *Routes of Drug Administration: Dosage, Design, and Pharmacotherapy Success*. in *ADME Processes in Pharmaceutical Sciences* (2018).

31. Kumar, G., Rao, V. & Kumar, N. *Development in efficacy assessment in relevant oncology models for breast cancer nanomedicine*. *Nanomedicines for Breast Cancer Theranostics* vol. 3 (Elsevier Inc., 2020).

32. Ruela, A. L. M., Perissinato, A. G., Lino, M. E. de S., Mudrik, P. S. & Pereira, G. R. Evaluation of skin absorption of drugs from topical and transdermal formulations. *Brazilian J. Pharm. Sci.* **52**, 527–544 (2016).

33. Homayun, B., Lin, X. & Choi, H. J. Challenges and recent progress in oral drug delivery systems for biopharmaceuticals. *Pharm.* **11**, (2019).

34. Bardal, S. K., Waechter, J. E. & Martin, D. S. Pharmacokinetics. in *Applied Pharmacology* 17–34 (2011).

35. Venkata, V. & Reddy, S. Importance of Selecting Route of Administration in Designing Products for Diabetic Foot Ulcers. *J. Pharm. Pharm.* **2**, 20–21 (2015).

36. Hua, S. Lipid-based nano-delivery systems for skin delivery of drugs and bioactives. *Integr. Regen. Pharmacol.* **30**, 219 (2015).

37. Neupane, R., Boddu, S. H. S., Renukuntla, J., Babu, R. J. & Tiwari, A. K. Alternatives to biological skin in permeation studies: Current trends and possibilities. *Pharm.* **12**, (2020).

38. Kahraman, E., Gungor, S. & Ozsoy, Y. Potential enhancement and targeting strategies of polymeric and lipid-based nanocarriers in dermal drug delivery. *Ther. Deliv.* **8**, 967–985 (2017).

39. Ng, K. W. & Lau, W. M. Skin Deep: The Basics of Human Skin Structure and Drug Penetration. in *Percutaneous Penetration Enhancers Chemical Methods in Penetration Enhancement* (eds. Dragicevic, N. & Maibach, H.) 3–11 (Springer US, 2015).

40. Mojumdar, E. H., Pham, Q. D., Topgaard, D. & Sparr, E. Skin hydration : interplay between molecular dynamics , structure and water uptake in the stratum corneum. *Sci. Rep.* **7**, 1–13 (2017).

41. Ali, S., Shabbir, M. & Shahid, N. The Structure of Skin and Transdermal Drug Delivery System - A Review. *Res. J. Pharm. Technol.* **8**, 3 (2016).

42. Bolzinger, M., Briançon, S., Pelletier, J. & Chevalier, Y. Penetration of drugs through skin, a complex rate-controlling membrane. *Curr. Opin. Colloid Interface Sci.* **17**, 156–165 (2012).

43. Bhowmick, M. & Sengodan, T. Mechanisms , kinetics and mathematical modelling of transdermal permeation - an updated review. *Int. J. Res. Dev. Pharm. Life Sci.* **2**, 636–641 (2013).

44. Sahle, F. F., Gebre-Mariam, T., Dobner, B., Wohlrab, J. & Neubert, R. H. H. Skin diseases associated with the depletion of stratum corneum lipids and stratum corneum lipid substitution therapy. *Skin Pharmacol. Physiol.* **28**, 42–55 (2015).

45. Davel, J. Topical delivery of niacinamide , encapsulated in niosome and proniosome carriers. (North-West University, 2016).

46. Segre, J. A. Epidermal barrier formation and recovery in skin disorders. *J. Clin. Invest.* **116**, 1150–1158 (2006).

47. Garg, A. *et al.* Psychological Stress Perturbs Epidermal Permeability Barrier Homeostasis. *Arch. Dermatol.* **137**, 53–59 (2001).

48. Donnelly, R. F. & Singh, T. R. R. *Novel Delivery Systems for Transdermal and Intradermal Drug Delivery*. in *Novel Delivery Systems for Transdermal and Intradermal Drug Delivery* (2015).

49. Plichta, J. K. *et al.* Local burn injury impairs epithelial permeability and antimicrobial peptide barrier function in distal unburned skin. *Crit. Care Med.* **42**, 420–431 (2014).

50. Thakur, R., Batheja, P., Kaushik, D. & Michniak, B. Structural and Biochemical Changes in Aging Skin and Their Impact on Skin Permeability Barrier. in *Skin Aging Handbook* 56–93 (2008).

51. Konda, S., Meier-Davis, S. R., Cayme, B., Jutaro, S. & Maibach, H. I. Age-related Percutaneous Penetration Part 1: Skin Factors. *Skin Therapy Lett.* **17**, (2012).

52. Di Cagno, M. P. *et al.* Experimental Determination of Drug Diffusion Coefficients in Unstirred Aqueous Environments by Temporally Resolved Concentration Measurements. *Mol. Pharm.* **15**, 1488–1494 (2018).

53. Shivakumar, H. N. & Murthy, S. N. CHAPTER 1 - Topical and Transdermal Drug Delivery. in *Handbook of Non-Invasive Drug Delivery Systems* (ed. Kulkarni, V. S.) 1–36 (2010).

54. Zhai, H. & Maibach, H. I. Effects of skin occlusion on percutaneous absorption: An overview. *Skin Pharmacol. Appl. Skin Physiol.* **14**, 1–10 (2001).

55. Ogawa-Fuse, C. *et al.* Impact of water exposure on skin barrier permeability and ultrastructure. *Contact Dermat. J.* **80**, (2018).

56. Zhai, H. & Maibach, H. I. Occlusion vs. skin barrier function. *Ski. Res. Technol.* **8**, 1–6 (2002).

57. Alkilani, A. Z., McCrudden, M. T. C. & Donnelly, R. F. Transdermal drug delivery: Innovative pharmaceutical developments based on disruption of the barrier properties of the stratum corneum. *Pharm.* **7**, 438–470 (2015).

58. Moribe, K. *et al.* Effect of particle size on skin permeation and retention of piroxicam in aqueous suspension. *Chem. Pharm. Bull.* **58**, 1096–1099 (2010).

59. Larrañeta, E., Lutton, R. E. M., Woolfson, A. D. & Donnelly, R. F. Microneedle arrays as transdermal and intradermal drug delivery systems: Materials science, manufacture and commercial development. *Mater. Sci. Eng. R Reports* **104**, 1–32 (2016).

60. N'Da, D. D. Prodrug strategies for enhancing the percutaneous absorption of drugs. *Molecules* J. **19**, 20780–20807 (2014).

61. Waters, L. J. & Bhuiyan, A. K. M. M. H. Ionisation effects on the permeation of pharmaceutical compounds through silicone membrane. *Colloids Surf. B: Biointer.* **141**, 553–557 (2016).

62. Forrester, J. V., Dick, A. D., McMenamin, P. G., Roberts, F. & Pearlman, E. General and ocular pharmacology. in *The Eye* (eds. Forrester, J. V., Dick, A. D., McMenamin, P. G., Roberts, F. & Pearlman, E.) 338–369 (2016).

63. Lau, E. Preformulation Studies. in *Handbook of Modern Pharmaceutical Analysis* (eds. Ahuja, S. & Scypinski, S.) 173–233 (2001).

64. Bhal, S. Log P — Making Sense of the Value. *Adv. Chem. Dev.* 1–4 (2007).

65. Offerta, A. *et al.* In vitro Percutaneous Absorption of Niacinamide and Phytosterols and in vivo Evaluation of their Effect on Skin Barrier Recovery. *Curr. Drug Deliv.* **13**, 111–120 (2016).

66. Thomas, S., Bharti, A., Tharpa, K. & Agarwal, A. Quantification of potential impurities by a stability indicating UV-HPLC method in niacinamide active pharmaceutical ingredient. *J. Pharm. Biomed. Anal.* **60**, 86–90 (2012).

67. Chen, A. C. & Damian, D. L. Nicotinamide and the skin. *Australas. J. Dermatol.* **55**, 169–175 (2014).

68. Fang, E. F. *et al.* NAD + in Aging : Molecular Mechanisms and Translational Implications. *Trends Mol. Med.* **23**, 899–916 (2017).

69. Gehring, W. Nicotinic acid / niacinamide and the skin. *J. Cosmet. Dermatol.* **3**, 88–93 (2004).

70. Bissett, D. L. Common cosmeceuticals. *Clin. Dermatol.* **27**, 435–445 (2009).

71. Gasperi, V., Sibilano, M., Savini, I. & Catani, M. V. Niacin in the central nervous system: An update of biological aspects and clinical applications. *Int. J. Mol. Sci.* **20**, 1–26 (2019).

72. PubChem Compound Summary for CID 936, Nicotinamide. *National Center for Biotechnology Information. Retrieved on February 1, 2021, from* https://pubchem.ncbi.nlm.nih.gov/compound/Nicotinamide.

73. Jacobs, S. Formulation , in vitro release and transdermal diffusion of salicylic acid and topical niacinamide. (North-West Universitu, Faculty of Health Sciences, 2009).

74. Scatozza, F. *et al.* Nicotinamide inhibits melanoma in vitro and in vivo. *J. Exp. Clin. Cancer Res.* **39**, 1–17 (2020).

75. Nikas, I. P., Paschou, S. A. & Ryu, H. S. The role of nicotinamide in cancer chemoprevention and therapy. *Biomol. J.* **10**, 1–20 (2020).

76. HM1, R. A review of nicotinamide: treatment of skin diseases and potential side effects. *J. Cosmet. Dermatol.* **13**, 324–328 (2014).

77. Forbat, E., Al-Niaimi, F. & Ali, F. R. Use of nicotinamide in dermatology. *Clin. Exp. Dermatol.* **42**, 137–144 (2017).

78. Harman, D. AGING: A THEORY BASED ON FREE RADICAL AND RADIATION CHEMISTRY. *J. Gerontol.* **11**, 298–300 (1956).

79. Pai, V. V, Shukla, P. & Kikkeri, N. N. Antioxidants in dermatology. *Indian Dermatol. Online J.* **5**, 210–214 (2014).

80. Sant, F. A. Antioxidants in dermatology *. *Brazilian Ann. Dermatology* **92**, 356–362 (2017).

81. Poljsak, B., Šuput, D. & Milisav, I. Achieving the Balance between ROS and Antioxidants : When to Use the Synthetic Antioxidants. *Oxid. Med. Cell. Longev.* **2013**, 11 (2013).

82. Kaur, I. P., Kapila, M. & Agrawal, R. Role of novel delivery systems in developing topical antioxidants as therapeutics to combat photoageing. *Ageing Res. Rev.* **6**, 271–288 (2007).

83. Farage, M. A., Miller, K. W., Elsner, P. & Maibach, H. I. Intrinsic and extrinsic factors in skin ageing : a review. *Int. J. Cosmet. Sci.* **30**, 87–95 (2008).

84. Zhang, S. & Duan, E. Fighting against Skin Aging : The Way from Bench to Bedside. *Cell Transplant*. **27**, 729–738 (2018).

85. Otlatıcı, G., Yeğen, G., Güngör, S. & Aksu, B. Overview on nanotechnology based cosmeceuticals to prevent skin aging. *Istanbul J. Pharm.* **48**, 55–62 (2018).

86. Ramos-e-Silva, M., Celem, L. R., Ramos-e-Silva, S. & Fucci-da-Costa, A. P. Anti-aging cosmetics: Facts and controversies. *Clin. Dermatol.* **31**, 750–758 (2013).

87. Hakozaki, T. *et al.* The effect of niacinamide on reducing cutaneous pigmentation and suppression of melanosome transfer. *Br. J. Dermatol.* **147**, 20–31 (2002).

88. Sinthupoom, N., Prachayasittikul, V., Prachayasittikul, S., Ruchirawat, S. & Prachayasittikul, V. Nicotinic acid and derivatives as multifunctional pharmacophores for medical applications. *Eur. Food Res. Technol.* **240**, 1–17 (2015).

89. Tanno, O., Ota, Y., Kitamura, N., Katsube, T. & Inoue, S. Nicotinamide increases biosynthesis of ceramides as well as other stratum corneum lipids to improve the epidermal permeability barrier. *Br. J. Dermatol.* **143**, 524–531 (2000).

90. Ghasemiyeh, P. & Samani, S. M. Hydrogels as Drug Delivery Systems; Pros and Cons (Review Article). *Trends Pharm. Sci.* **5**, 7–24 (2019).

91. Wang, W., Narain, R. & Zeng, H. Hydrogels. in *Polymer Science and Nanotechnology* 203–244 (2020).

92. Varaprasad, K., Malegowd, G., Jayaramudu, T., Mohan, M. & Sadiku, R. A mini review on hydrogels classi fi cation and recent developments in miscellaneous applications. *Mater. Sci. Eng. C* **79**, 958–971 (2017).

93. Bahram, M., Mohseni, N. & Moghtader, M. An Introduction to Hydrogels and Some Recent Applications. in *Emerging Concepts in Analysis and Applications of Hydrogels* 9–38 (2016).

94. Chai, Q., Jiao, Y. & Yu, X. Hydrogels for Biomedical Applications : Their Characteristics and the Mechanisms behind Them. *Gels* **3**, 15 (2017).

95. Zhang, Y. *et al.* Physically crosslinked poly(vinyl alcohol)-carrageenan composite hydrogels: Pore structure stability and cell adhesive ability. *R. Soc. Chem. Adv.* **5**, 78180–78191 (2015).

96. Frias, A. M. *et al.* Carrageenan-Based Hydrogels for the Controlled Delivery of PDGF-BB in Bone Tissue Engineering Applications. *Biomacromolecules.* **10**, 1392–1401 (2009).

97. Akalin, G. O. & Pulat, M. Preparation and characterization of κ-carrageenan hydrogel for controlled release of copper and manganese micronutrients. *Polym. Bull.* **77**, 1359–1375 (2020).

98. Mihaila, S. M. *et al.* Photocrosslinkable kappa-carrageenan hydrogels for tissue engineering applications. *Adv. Healthc. Mater.* **2**, 895–907 (2013).

99. Mangione, M. R. *et al.* K + and Na + effects on the gelation properties of κ-Carrageenan. *Biophys. Chem.* **113**, 129–135 (2005).

100. Liu, S., Huang, S. & Li, L. Thermoreversible gelation and viscoelasticity of κ − carrageenan hydrogels. *J. Rheol. (N. Y. N. Y).* **60**, 203–214 (2016).

101. Mitura, S., Sionkowska, A. & Jaiswal, A. Biopolymers for hydrogels in cosmetics: review. *J. Mater. Sci. Mater. Med.* **31**, (2020).

102. Song, C. K. *et al.* A novel vesicular carrier , transethosome , for enhanced skin delivery of voriconazole : Characterization and in vitro / in vivo evaluation. *Colloids Surf. B: Biointer.* **92**, 299–304 (2012).

103. Moolakkadath, T. *et al.* Development of transethosomes formulation for dermal fisetin delivery : Box – Behnken design , optimization , in vitro skin penetration , vesicles – skin interaction and dermatokinetic studies. *Artif. Cells, Nanomedicine, Biotechnol.* **46**, S755–S765 (2018).

104. Mishra, K. K., Kaur, C. D., Verma, S. & Sahu, A. K. Transethosomes and Nanoethosomes : Recent Approach on Transdermal Drug Delivery System. in *International Journal of Nanomedicine* vol. 14 1953–1968 (2019).

105. Abdelbary, A. A. & Refai, H. Use of transethosomes for enhancing the transdermal delivery of olmesartan medoxomil : in vitro , ex vivo , and in vivo evaluation. *Int. J. Nanomedicine* **14**, 1953–1968 (2019).

106. Shaji, J. & Bajaj, R. TRANSETHOSOMES: A NEW PROSPECT FOR ENHANCED TRANSDERMAL DELIVERY. *Int. J. Pharm. Sci. Res.* **9**, 2681–2685 (2018).

107. Kumar, L., Verma, S., Aktuelno, T. T., Singh, K. & Prasad, D. N. Ethanol Based Vesicular Carriers in Transdermal Drug Delivery: Nanoethosomes and Transethosomes in Focus. *NanoWorld J.* **2**, 41–51 (2016).

108. Sala, M., Diab, R., Elaissari, A. & Fessi, H. Lipid nanocarriers as skin drug delivery systems : Properties , mechanisms of skin interactions and medical applications. *Int. J. Pharm.* **535**, 1–17 (2018).

109. Apsara, S., Opatha, T., Titapiwatanakun, V. & Chutoprapat, R. Transfersomes : A Promising Nanoencapsulation Technique for Transdermal Drug Delivery. *Pharm.* **12**, 855 (2020).

110. Lee, M. H. *et al.* In vivo anti-melanogenesis activity and in vitro skin permeability of niacinamide-loaded flexible liposomes (Bounsphere^{TM}). *J. Drug Deliv. Sci. Technol.* **31**, 147–152 (2016).

111. Shin, C. I., Kim, M. & Kim, Y. C. Delivery of niacinamide to the skin using microneedle-like particles. *Pharm.* **11**, (2019).

112. Yeo, S., An, J., Park, C., Kim, D. & Lee, J. Design and characterization of phosphatidylcholine-based solid dispersions of aprepitant for enhanced solubility and dissolution. *Pharm.* **12**, 407 (2020).

113. Skoog, D. A. & West, D. M. *Principles of Instrumental Analysis*. (Thomson Learning, 1992).

114. Smith, G. European medicines agency guideline on bioanalytical method validation: What more is there to say? *Bioanalysis* **4**, 865–868 (2012).

115. Gaikwad, V. L., Choudhari, P. B., Bhatia, N. M. & Bhatia, M. S. Characterization of pharmaceutical nanocarriers: in vitro and in vivo studies. in *Nanomaterials for Drug Delivery and Therapy* 33–58 (Elsevier Inc., 2019).

116. Massella, D., Celasco, E., Salaün, F., Ferri, A. & Barresi, A. A. Overcoming the limits of flash nanoprecipitation: Effective loading of hydrophilic drug into polymeric nanoparticles with controlled structure. *Polymers (Basel).* **10**, (2018).

117. Kudo, M., Katayoshi, T., Kobayashi-Nakamura, K., Akagawa, M. & Tsuji-Naito, K. H+/peptide transporter (PEPT2) is expressed in human epidermal keratinocytes and is involved in skin oligopeptide transport. *Biochem. Biophys. Res. Commun.* **475**, 335–341 (2016).

118. Moosavi, S. M. & Ghassabian, S. Linearity of Calibration Curves for Analytical Methods: A Review of Criteria for Assessment of Method Reliability. in *Calibration and Validation of Analytical Methods - A Sampling of Current Approaches* 110–127 (2018).

119. Segundo, M. A. *et al.* Development and validation of HPLC method with fluorometric detection for quantification of bisnaphthalimidopropyldiaminooctane in animal tissues following administration in polymeric nanoparticles. *J. Pharm. Biomed. Anal.* **120**, 290–296 (2016).

120. Sharadha, M., Gowda, D. V., Vishal Gupta, N. & Akhila, A. R. An overview on topical drug delivery system – updated review. *Int. J. Res. Pharm. Sci.* **11**, 368–385 (2020).

121. Hu, W., Wang, Z., Xiao, Y., Zhang, S. & Wang, J. Advances in crosslinking strategies of biomedical hydrogels. *Biomater. Sci.* **7**, 843–855 (2019).

122. Sharma, A., Bhat, S., Vishnoi, T., Nayak, V. & Kumar, A. Three-dimensional supermacroporous carrageenan-gelatin cryogel matrix for tissue engineering applications. *Biomed Res. Int.* 1–15 (2013).

123. Li, Z. & Lin, Z. Recent advances in polysaccharide-based hydrogels for synthesis and applications. *Aggregate J.* 1–26 (2021).

124. Rodrigues, S., Costa, A. M. R. Da & Grenha, A. Chitosan/carrageenan nanoparticles: Effect of cross-linking with tripolyphosphate and charge ratios. *Carbohydr. Polym.* **89**, 282–289 (2012).

125. Beneke, C. E., Viljoen, A. M. & Hamman, J. H. Polymeric plant-derived excipients in drug delivery. *Molecules J.* **14**, 2602–2620 (2009).

126. Gajra, B. *et al.* Poly vinyl alcohol hydrogel and its pharmaceutical and biomedical applications: A review. *Int. J. Pharm. Res.* **4**, 20–26 (2012).

127. Franco, P. & De Marco, I. The use of poly(N-vinyl pyrrolidone) in the delivery of drugs: A review. *Polymers (Basel).* **12**, 18–21 (2020).

128. Kulkarni, V. S. & Shaw, C. Use of Polymers and Thickeners in Semisolid and Liquid Formulations. in *Essential Chemistry for Formulators of Semisolid and Liquid Dosages* 43–69 (2016).

129. Herman, A. & Herman, A. P. Essential oils and their constituents as skin penetration enhancer for transdermal drug delivery: A review. *J. Pharm. Pharmacol.* **67**, 473–485 (2015).

130. Aggarwal, G., Dhawan, S. & L. HariKumar, S. Natural Oils as Skin Permeation Enhancers for Transdermal Delivery of Olanzapine: In Vitro and In Vivo Evaluation. *Curr. Drug Deliv.* **9**, 172–181 (2012).

131. Arockia Mary, I. *et al.* Lithium ion conducting membrane based on K-carrageenan complexed with lithium bromide and its electrochemical applications. *Ionics (Kiel).* **25**, 5839–5855 (2019).

132. Rahma, A. *et al.* Intermolecular Interactions and the Release Pattern of Electrospun Curcumin-Polyvinyl(pyrrolidone) Fiber. *Biol. Pharm. Bull.* **39**, 163–173 (2016).

133. Erizal, E., Tjahyono, T., Perkasa, D. P. & Darwis, D. Synthesis of Polyvinyl Pirrolidone (PVC) /K-Carrageenan Hydrogel Prepared by Gamma Radiation Processing As a Function of Dose and PVP Concentration. *Indones. J. Chem.* **13**, 41–46 (2013).

134. Bayarı, S. & Atac, A. Coordination behaviour of nicotinamide : an infrared spectroscopic study. *J. Mol. Struct.* **655**, 163–170 (2003).

135. Moraes, L. G. P. *et al.* Infrared spectroscopy: A tool for determination of the degree of conversion in dental composites. *J. Appl. Oral Sci.* **16**, 145–149 (2008).

136. Yacob, N. & Hashim, K. Morphological effect on swelling behaviour of hydrogel. *AIP Conf. Proc.* **1584**, 153–159 (2014).

137. Rodrigues, M. T., Carvalho, P. P., Gomes, M. E. & Reis, R. L. Biomaterials in Preclinical Approaches for Engineering Skeletal Tissues. in *Translational Regenerative Medicine* 127–139 (Elsevier Inc., 2015).

138. Necas, J. & Bartosikova, L. Carrageenan: A review. *Vet. Med. (Praha).* **58**, 187–205 (2013).

139. Ako, K. Influence of elasticity on the syneresis properties of κ-carrageenan gels. *Carbohydr. Polym.* **115**, 408–414 (2015).

140. North, T. & Wales, E. Properties of Individual Gums. *Encyclopedia of Food Sciences and Nutrition (Seccind Edition)* 2992–3001 (2003).

141. Mohammed, D., Matts, P. J., Hadgraft, J. & Lane, M. E. In vitro-in vivo correlation in skin permeation. *Pharm. Res.* **31**, 394–400 (2014).

142. Zhang, Y. *et al*. A comparison of the in vitro permeation of niacinamide in mammalian skin and in the Parallel Artificial Membrane Permeation Assay (PAMPA) model. *Int. J. Pharm.* **556**, 142–149 (2019).

143. Haque, T., Lane, M. E., Sil, B. C., Crowther, J. M. & Moore, D. J. In vitro permeation and disposition of niacinamide in silicone and porcine skin of skin barrier-mimetic formulations. *Int. J. Pharm.* **520**, 158–162 (2017).

144. Touitou, E., Godin, B., Karl, Y., Bujanover, S. & Becker, Y. Oleic acid, a skin penetration enhancer, affects Langerhans cells and corneocytes. *J. Control. Release* **80**, 1–7 (2002).

145. Jenning, V., Gysler, A., Schäfer-Korting, M. & Gohla, S. H. Vitamin A loaded solid lipid nanoparticles for topical use: Occlusive properties and drug targeting to the upper skin. *Eur. J. Pharm. Biopharm.* **49**, 211–218 (2000).

146. Danaei, M. *et al*. Impact of particle size and polydispersity index on the clinical applications of lipidic nanocarrier systems. *Pharmaceutics* **10**, 1–17 (2018).

147. Lin, P. C., Lin, S., Wang, P. C. & Sridhar, R. Techniques for physicochemical characterization of nanomaterials. *Biotechnol. Adv.* **32**, 711–726 (2014).

148. Upadhyay, S. U., Patel, J. K., Patel, V. A. & Saluja, A. K. Effect of different lipids and surfactants on formulation of solid lipid nanoparticles incorporating tamoxifen citrate. *J. Pharm. Bioallied Sci.* **4**, 112–113 (2012).

149. Sis, H. & Birinci, M. Effect of nonionic and ionic surfactants on zeta potential and dispersion properties of carbon black powders. *Colloids Surfaces A Physicochem. Eng. Asp.* **341**, 60–67 (2009).

150. Gusain, R. & Khatri, O. P. Fatty acid ionic liquids as environmentally friendly lubricants for low friction and wear. *RSC Adv.* **6**, 3462–3469 (2016).

151. Tazina, E. V., Kostin, K. V. & Oborotova, N. A. Specific features of drug encapsulation in liposomes (A review). *Pharm. Chem. J.* **45**, 481–490 (2011).

152. Colletier, J. P., Chaize, B., Winterhalter, M. & Fournier, D. Protein encapsulation in liposomes: Efficiency depends on interactions between protein and phospholipid bilayer. *BMC Biotechnol.* **2**, 1–8 (2002).

153. Almgren, M. & Edwards, K. Cryo transmission electron microscopy of liposomes and related structures. *Physicochem. Eng. Asp.* **174**, 3–21 (2008).

154. Ascenso, A. *et al*. Development, characterization, and skin delivery studies of related ultradeformable vesicles: Transfersomes, ethosomes, and transethosomes. *Int. J. Nanomedicine* **10**, 5837–5851 (2015).

7. Supplementary Figures

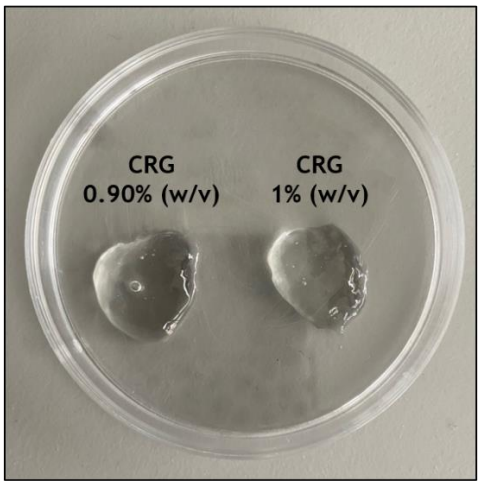


Figure S1 – Hydrogels with different CRG amounts, 0.90% and 1% (w/v).

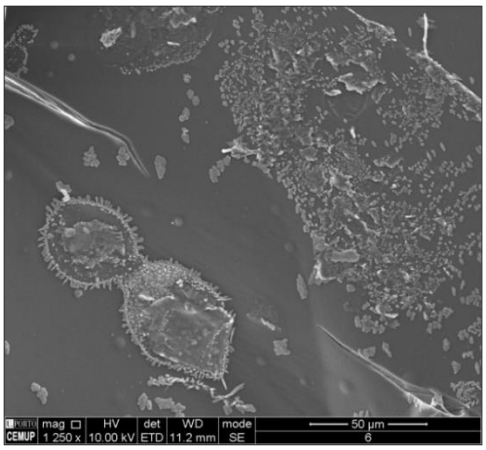


Figure S2 – Artifacts on the surface of CRG-PVP hydrogel matrix (×1250 magnification).

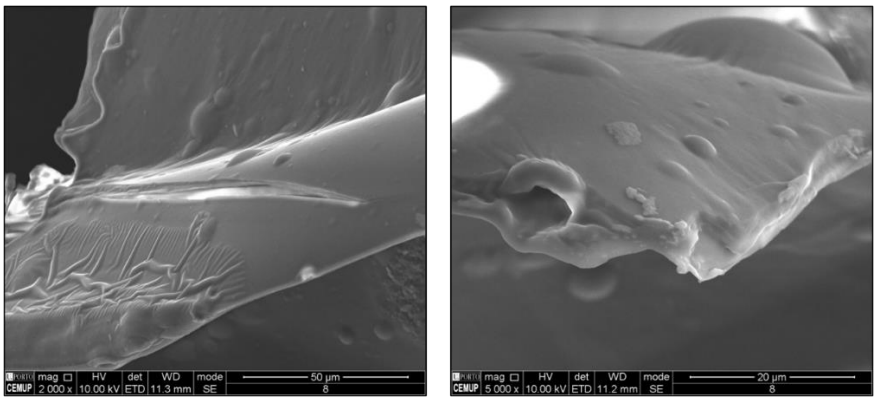


Figure S3 - JO silk-like effect on CRG-PVP hydrogel macrostructure. CRG-PVP NIA-loaded hydrogel w/ 0.5% of JO (SEM, ×2000 and ×5000 magnification, respectively).

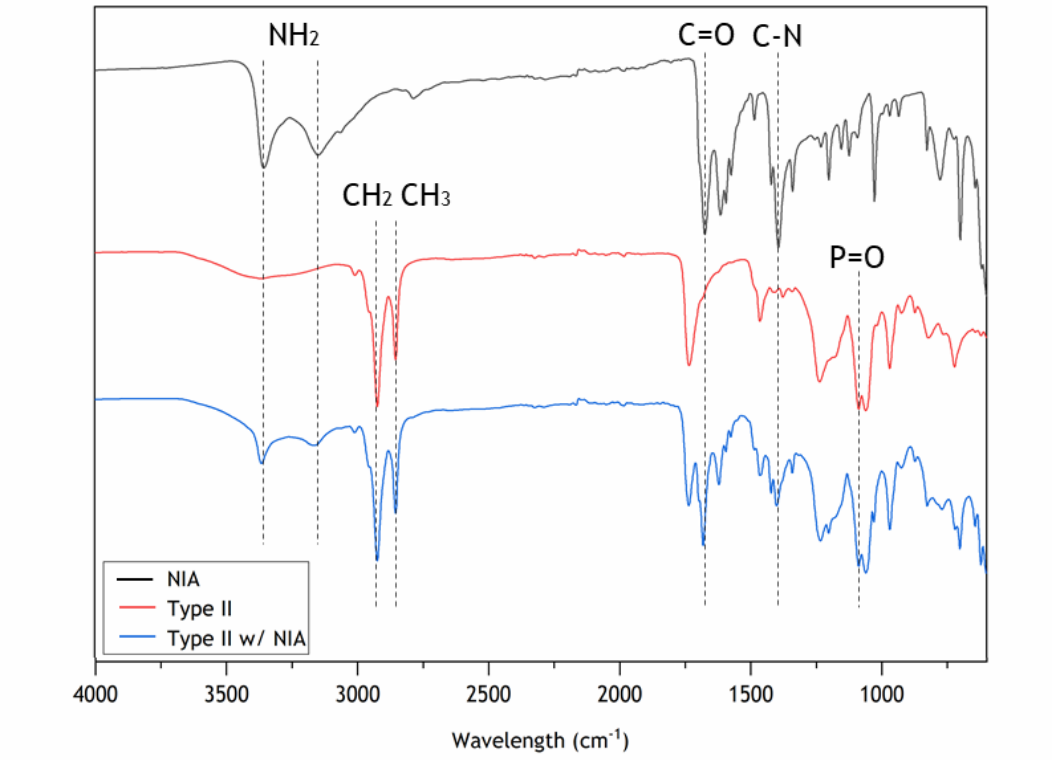


Figure S4 - The FTIR spectra of reference compound (NIA) and nanoformulations (Type II and Type II w/ NIA).

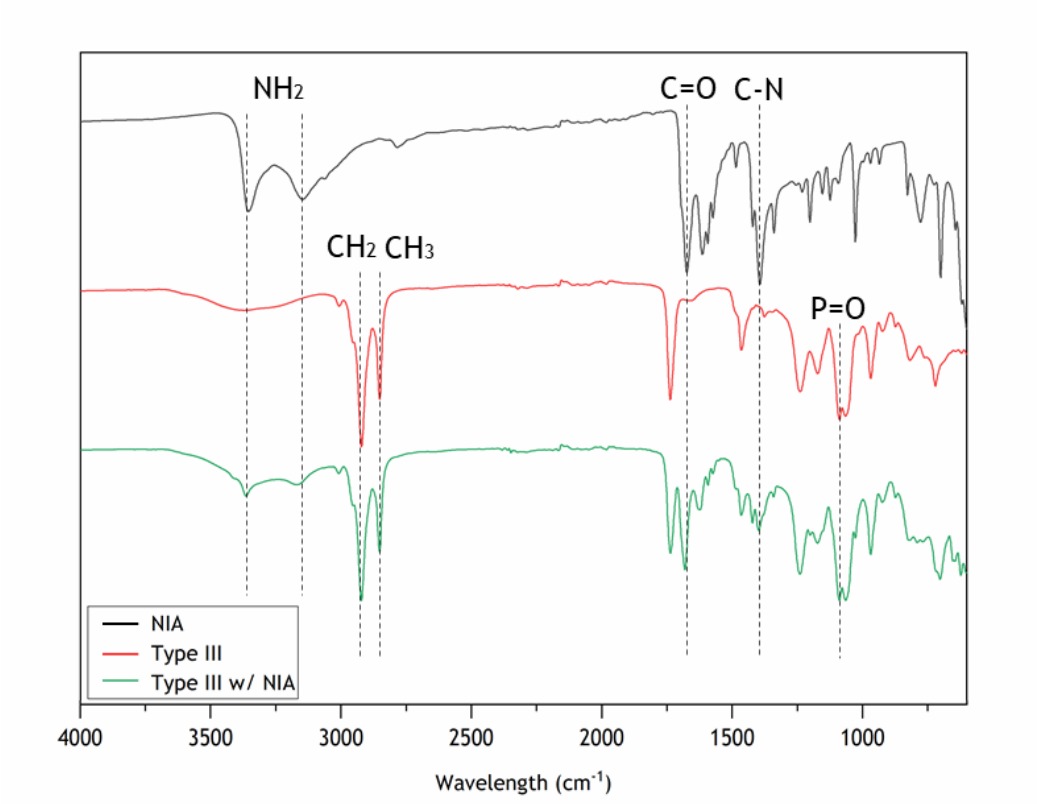


Figure S5 - The FTIR spectra of reference compound (NIA) and nanoformulations (Type III and Type III w/ NIA).

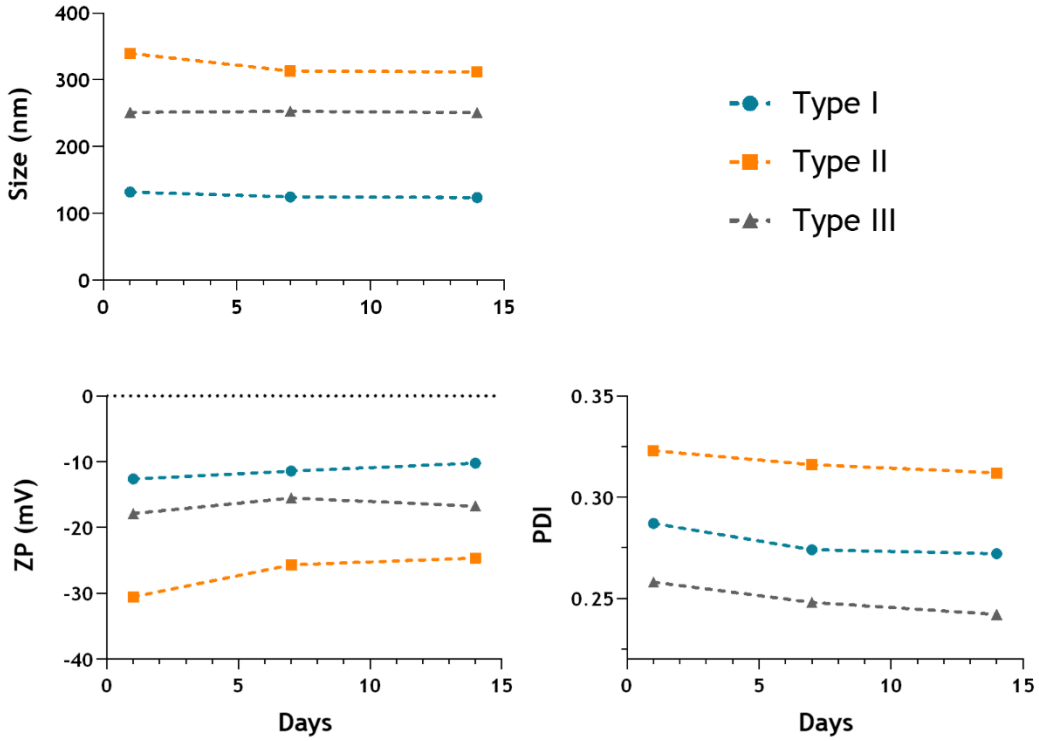


Figure S6 - Storage stability of non-loaded formulations at 4°C over 2 weeks. Size, zeta potential and polydispersity index values displayed (Size: SD<6%; ZP: SD<10%; PDI: SD<7%).